npj | biofilms and microbiomes

Article

Published in partnership with Nanyang Technological University

https://doi.org/10.1038/s41522-025-00712-y

Akkermansia muciniphila ameliorates doxorubicin-induced cardiotoxicity by regulating PPARα-dependent mitochondrial biogenesis

Hui Lin[1,12], Xian Shao[2,12], Haodi Gu[3], Xinrou Yu[4], Lingyan He[5], Jiedong Zhou[6], Zuoquan Zhong[7], Shitian Guo[8], Dan Li[9], Fei Chen[10], Yongfei Song[1], Lili Xu[2], Ping Wang[11], Liping Meng[11,13] ✉, Jufang Chi[4,13] ✉ & Jiangfang Lian[1,13] ✉

Doxorubicin (DOX) is a key chemotherapeutic agent but is also a leading cause of DOX-induced cardiotoxicity (DIC), limiting its clinical use. *Akkermansia muciniphila* (*A. muciniphila*), known for its benefits as a probiotic in treating metabolic syndrome, has uncertain effects in the context of DIC. Here, 16S rRNA sequencing of fecal samples from anthracycline-treated patients and DIC mice revealed marked depletion of *A. muciniphila*. Cardiac transcriptomics, supported by in vitro experiments, showed that *A. muciniphila* colonization improved mitochondrial function and alleviated DIC by activating the PPARα/PGC1α signaling pathway in both normal and antibiotic-treated C57BL/6 mice. Further analysis uncovered a restructured microbiome–metabolome network following *A. muciniphila* administration, which contributed to DIC protection. Notably, *A. muciniphila* supplementation increased serum levels of the tryptophan metabolite indole-3-propionic acid (IPA), which binds to the cardiac aryl hydrocarbon receptor (AhR), leading to the activation of the PPARα/PGC1α signaling pathway. In conclusion, our study sheds light on the potential of *A. muciniphila* as a probiotic in mitigating DIC.

Doxorubicin (DOX) is a widely used anthracycline chemotherapy drug for treating various cancers, including breast cancer and leukemia. However, its efficacy is limited by cardiotoxicity, a significant long-term side effect that increases morbidity and mortality among cancer survivors[1]. DOX-induced cardiotoxicity (DIC) largely depends on the method of administration, the cumulative duration of chemotherapy, and the specific dosage regimen[2]. Approximately 20% of cancer survivors in Europe exhibit a reduction in cardiac function without symptoms, and this percentage is notably higher among those who survived cancer during childhood[3]. Doxorubicin forms an irreversible complex, leading to the impairment of mitochondrial membrane potential. This makes the mitochondria more vulnerable to reactive oxygen species, resulting in the inhibition of the mitochondrial respiratory chain[4] and subsequent mitochondrial bioenergetics disorder[5]. Impaired mitochondrial energetics and cardiac fibrosis contribute to the onset and progression of heart failure[6]. Hence, identifying preventive and therapeutic strategies against mitochondrial bioenergetics

[1]Department of Cardiology, The Affiliated Lihuili Hospital of Ningbo University, Ningbo, China. [2]Medical Research Center, Shaoxing People's Hospital, Shaoxing, China. [3]College of Medicine, Shaoxing University, Shaoxing, China. [4]Department of Cardiology, Zhuji Affiliated Hospital of Wenzhou Medical University, Shaoxing, China. [5]Department of Traditional Chinese Medicine, Shaoxing People's Hospital, Zhejiang University Shaoxing Hospital, Shaoxing, China. [6]Cardiac Arrhythmia Center, The First Affiliated Hospital of Ningbo University, Ningbo, China. [7]Department of Respiratory Medicine, Shaoxing People's Hospital (Shaoxing Hospital, Zhejiang University School of Medicine), Shaoxing, China. [8]Department of Cardiology, The Second Affiliated Hospital, Zhejiang University School of Medicine, Hangzhou, China. [9]Department of Haematology, Shaoxing People's Hospital (Shaoxing Hospital, Zhejiang University School of Medicine), Shaoxing, China. [10]Department of General Surgery (Breast and Thyroid Surgery), Shaoxing People's Hospital (Shaoxing Hospital, Zhejiang University School of Medicine), Shaoxing, China. [11]Department of Cardiology, Shaoxing People's Hospital (Shaoxing Hospital, Zhejiang University School of Medicine), Shaoxing, China. [12]These authors contributed equally: Hui Lin, Xian Shao.[13]These authors jointly supervised this work: Liping Meng, Jufang Chi, Jiangfang Lian. ✉e-mail: Mengliping@zju.edu.cn; jf_chi@163.com; hjmpin@163.com

disorder is crucial for addressing DIC by investigating the molecular mechanisms that drive DIC.

The gut microbiome, which constitutes the second-largest genome in the host, plays a significant role in cardiac injury and heart failure. Notably, the composition of gut microbiota varies in patients with breast cancer[7], and fecal microbiota transplantation (FMT) is able to increase DOX responsiveness of triple-negative breast cancer cells[8,9]. Our previous study also confirmed that FMT alleviated DIC by regulating cardiac mitochondrial fission and fusion[10]. Specific genera, *Faecalibaculum*, *Dubosiella*, and *Lachnospiraceae* were increased, while *Allobaculum*, *Muribaculum*, and *Lachnoclostridium* were decreased in mice with DIC[11]. Although doxorubicin-induced gut microbiota dysbiosis has been documented[12], no studies have yet explored the impact of supplementing with specific intestinal bacteria on DIC. The specific bacterial components and the detailed underlying mechanisms remain unclear. As a result, the current understanding of the gut microbiota in DIC is quite limited.

Uncovering the mechanism by which gut microbiota influences cardiac fibrosis would be beneficial for the development of gut microbiota-based therapeutics in DIC. By using 16S RNA sequencing, we first described the alteration of gut microbiota in DIC mice, in a time-dependent manner. Our findings revealed that *Akkermansia muciniphila* (*A. muciniphila*) was notably and stably decreased in breast cancer patients and C57BL/6 mice treated with anthracycline. *A. muciniphila* supplementation restored DOX-induced gut microbiota dysbiosis and intestinal epithelial barrier. *A. muciniphila* increased circulating indole-3-propionic acid (IPA) levels to attenuate DOX-induced diastolic dysfunction, cardiac fibrosis, and mitochondrial bioenergetics disorder. Administration of IPA leads to increased electron transport chain (ETC) activity by binding cardiac aryl hydrocarbon receptor (AhR) and subsequent activation of peroxisome proliferator-activated receptor α (PPARα) signaling pathway. These findings provide a therapeutic strategy for DIC through supplementation with *A. muciniphila*.

Results

The abundance of *A. muciniphila* is decreased in breast cancer patients treated with anthracycline-based chemotherapy and in C57/BL6 mice with DIC

Firstly, we enrolled 30 patients with breast cancer who were subjected to either anthracycline-based chemotherapy (AC group) or non-anthracycline-based chemotherapy (nAC group). The results of principal coordinate analysis (PCoA) demonstrated distinct clustering between the AC and nAC groups (Fig. 1a). At the genus level, the *A. muciniphila* abundance was significantly decreased in the AC group compared to the nAC group (Fig. 1b, c). Receiver operating characteristic (ROC) analysis showed that *A. muciniphila* had a high discriminatory power in clinically identifying the use of anthracycline (Fig. 1d). To further investigate the relationship between the gut microbiota and DIC progression, we compared fecal samples from four-paired mice treated with DOX for continuous 4 weeks by 16S rRNA gene sequencing. The data showed that DOX had no influence on the α diversity of the gut microbiota (Supplementary Fig. 1a). PCoA analysis identified the clustering between DOX groups with different intervention times (Fig. 1e, f). At the phylum level, with increasing duration of DOX, the abundance of *Verrucomicrobiota* was decreased, whereas *Actinobacteriota* was increased (Supplementary Fig. 1b). The Venn diagram showed 930, 2055, 1773, and 1167 operational taxonomic units (OTUs) at the genus level in the DOX groups from week 0 to 4, respectively, with 292 OTUs among the groups (Supplementary Fig. 1c). At the genus level, DOX deposition caused decreased the abundance of *A. muciniphila*, *HT002*, *Desulfovibrio* and *Olsenella*, while increased the abundance of *Bifidobacterium*, *Arthrobacter*, *Turicibacter* and *Staphylococcus*. Notably, the abundance of *A. muciniphila* decreased from the second week and continued until the fourth week (Fig. 1g, h), leading us to assume it as a probiotic and exert a protective role in the progression of DIC. Subsequent linear discriminant analysis effect size (LEfSe) analysis identified a total of 25 differentially abundant taxa across all taxonomic levels, from phylum to genus (LDA > 4, $p < 0.05$, Supplementary Fig. 1c, d). Interestingly, *A. muciniphila* was positively correlated with the cardiac function including left ventricular ejection fraction (LVEF) and left ventricular fraction shortening (LVFS), and indicator of cardiac hypertrophy heart weight/body weight, and negatively correlated with the cardiac injury indexes, including lactate dehydrogenase (LDH) and creatine phosphokinase-MB isoenzyme (CK-MB) (Fig. 1i). The PICRUSt2 analysis indicated that glycogen biosynthesis, NAD salvage pathway, and L-histidine degradation I were the three main pathways involved in the function of altered microbiota under DOX stimulation (Fig. 1j).

A. muciniphila supplementation improves DIC in mice

Our previous studies have found that administration of an antibiotic cocktail caused loss of gut microbiota, which aggravates DIC[13]; whereas FMT from healthy mice attenuates DIC[10], indicating that gut microbiota play a vital role in DIC. To explore the effect of *A. muciniphila* on DIC, we fed male DIC mice with *A. muciniphila* during a 4-week-long modeling. Furthermore, benzydamine (an effective *A. muciniphila* inhibitor approved by Nie et al.[14]) was used to inhibit the colonization of *A. muciniphila* (Supplementary Fig. 2). *A. muciniphila*-colonized mice had increased LVEF and LVFS, reduced CK-MB and LDH compared with the DOX-treated mice, whereas the addition of Ben abolished the cardioprotective of *A. muciniphila* (Supplementary Fig. 3a–e). Additionally, *A. muciniphila* supplementation alleviated DOX-induced cardiac injury, atrophy, and fibrosis. The effects of *A. muciniphila* on cardiac pathological changes were disappearing in the *A. muciniphila* plus Ben group (Supplementary Fig. 3f–j). Accumulation of extracellular matrix (ECM) leads to impaired systolic and diastolic function, and *A. muciniphila* treatment reduced the ECM-related protein, smooth muscle actin (SMA), collagen III, and collagen III in DIC mice. The ECM-related proteins were again increased in the mice from the *A. muciniphila* plus Ben group when compared to the *A. muciniphila* group (Supplementary Fig. 3k–n). Moreover, we confirmed that administration of Ben did not exhibit any cardiac toxicity in C57BL/6 mice or in mice with DIC (Supplementary Fig. 4). To evaluate whether *A. muciniphila* contributes to cardio-protection independently of complex microbiota interactions, mice were pretreated with broad-spectrum antibiotics (Abx) to deplete commensal bacteria (Supplementary Fig. 5). Following colonization with *A. muciniphila*, the expression of *A. muciniphila* was markedly increased (Fig. 2a). The results of echocardiography showed that *A. muciniphila* in parallel with Abx administration significantly rescued the reduction of LVEF and LVFS induced by DOX (Fig. 2b–d). In addition, *A. muciniphila* reconstitution reduced the levels of cardiac injury markers (CK-MB and LDH) in DIC mice (Fig. 2e, f). Histological analysis showed that the heart from the DIC mice displayed decreased cardiomyocyte size and increased myocardial fibrosis compared with Abx mice, whereas these effects were greatly alleviated by *A. muciniphila* colonization (Fig. 2h–k). Immunofluorescence staining revealed that DOX treatment resulted in the accumulation of collagen (increased fluorescence intensity of SMA and collagen III), whereas *A. muciniphila* significantly reduced collagen deposition (Fig. 2l). Subsequent western blot analysis confirmed that *A. muciniphila* treatment reversed DOX-induced increase in ECM-related protein, SMA, collagen I, and collagen III (Fig. 2m). Above data indicated that *A. muciniphila* colonization significantly alleviated DOX-induced cardiomyopathy in mice.

A. muciniphila supplementation improves DIC by regulating mitochondrial bioenergetics

To elucidate the mechanisms by which *A. muciniphila* ameliorates DIC, we performed RNA-seq analysis on heart tissues stimulated with DOX. This analysis identified 423 upregulated and 1260 downregulated differentially expressed genes (DEGs, defined using log 2-fold change >1 and p value < 0.05; Supplementary Fig. 6a) in DIC and *A. muciniphila*-treated hearts. The heatmap and volcano plot illustrating these DEGs are presented in Supplementary Fig. 6b–d. Comparative KEGG pathway analysis and Gene Set Enrichment Analysis (GSEA) indicated that these DEGs are significantly enriched in mitochondrial metabolic pathways (Fig. 3a and

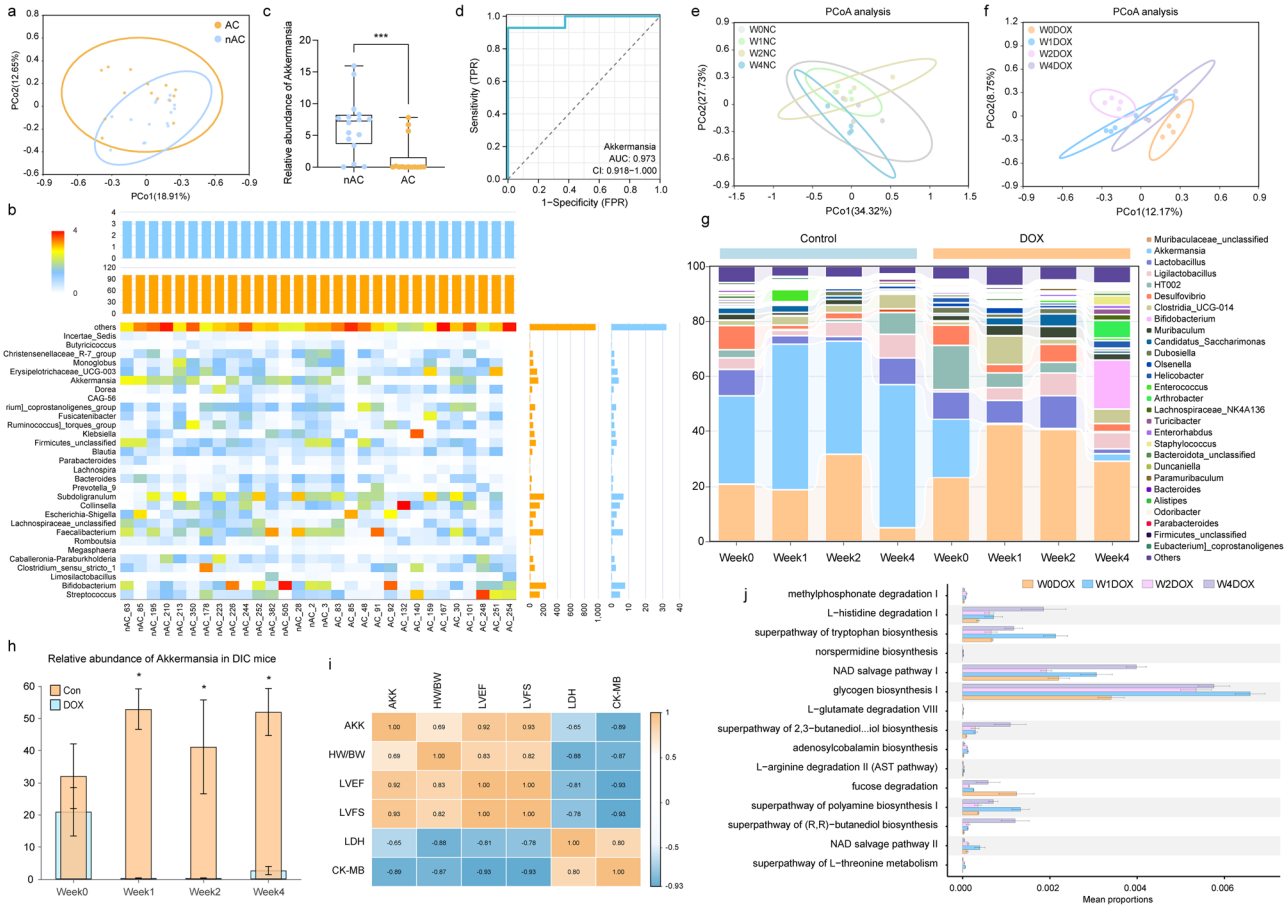

Fig. 1 | *Akkermansia muciniphila* (*A. muciniphila*) was depleted in C57BL/6 mice subjected to doxorubicin (DOX) and in breast cancer patients treated with anthracycline-based chemotherapy. a Principal component analysis (PCA) score plot for the feces metabolome of breast cancer patients with or without anthracycline (AC, $n = 14$) or other chemotherapy therapy (nAC, $n = 16$). Each point represented a sample. **b** At the genus level, a heatmap showed the relative abundance of bacteria in breast cancer patients from AC ($n = 14$) and nAC groups ($n = 16$). **c** Relative abundance of *A. muciniphila* in the AC and nAC groups. **d** Receiver operating characteristic analysis with the area under curve (AUC) is used to determine the efficiency of *A. muciniphila* in distinguishing anthracycline utilization ($n = 30$). **e**, **f** PCA score plot for the feces metabolome of control mice (**e**) and DOX-treated mice (**f**) at the indicated time ($n = 4$). **g** At the genus level, relative abundance of bacteria (percentage of total bacteria) in mice treated with or without DOX at the indicated time (week0: before DOX administration; week1–4: on the first day following DOX administration during the specified week). Different colors represent different bacteria at the same level ($n = 4$). **h** Relative abundance of *A. muciniphila* in mice from the control and DOX groups ($n = 4$). **i** Pearson's correlation analysis between *A. muciniphila* levels and cardiac injury markers of mice, including heart weight (HW)/(body weight) BW, LVEF, LVFS, serum lactate dehydrogenase (LDH), and creatine kinase-MB (CK-MB) ($n = 4$). **j** Prediction of altered KEGG pathways using PICRUSt2 analysis of the fecal microbiota for DOX groups at the indicated time. Data are presented as the mean ± SD. $^{*}P < 0.05$, $^{***}P < 0.001$.

Supplementary Fig. 7a). Specifically, oxidative phosphorylation (Supplementary Fig. 7b) was among the top three enriched KEGG pathways and exhibited a negative correlation with *A. muciniphila* treatment (Fig. 3a). Consistent with the KEGG pathway analysis, a broad downregulation of mitochondrial respiratory ETC genes was observed in DIC hearts, which was reversed by *A. muciniphila* treatment (Fig. 3b). To validate these findings, we evaluated the effects of *A. muciniphila* on the activity of mitochondrial respiratory chain complexes I–V. As shown in Fig. 3c, DOX significantly disrupted the functions of complexes I and V; however, the addition of *A. muciniphila* reversed these effects caused by DOX. To corroborate these findings, we evaluated the in vivo protein expression of ETC complex subunits. Consistent with our expectations, the expression levels of ETC complex proteins (Ndufb8, Sdhb, Mtco1, and Atp5a) were significantly reduced in DOX-stimulated hearts compared to control hearts. Conversely, these ETC proteins were markedly upregulated in the *A. muciniphila*-treated hearts relative to the DOX group (Fig. 3d). To further substantiate the impact of *A. muciniphila* on mitochondrial bioenergetics, the supernatant of *A. muciniphila* was utilized to treat DOX-exposed H9C2 cells. The *A. muciniphila* supernatant displayed significant toxicity to H9C2 cells when its concentration exceeded 16% and 2–8% concentration of *A. muciniphila* supernatant was able to protect H9C2 cells from DOX-induced toxicity (Supplementary Fig. 8a, b). Following DOX treatment, both ATP levels and the JC-1 ratio were reduced. However, the *A. muciniphila* supernatant demonstrated an ameliorative effect on mitochondrial function by enhancing mitochondrial membrane potential and ATP synthesis (Supplementary Fig. 8c–e). Subsequently, we employed extracellular flux analysis to monitor mitochondrial respiratory capacity in real-time. DOX significantly diminished both basal and maximal respiration. In contrast, treatment with *A. muciniphila* supernatant restored mitochondrial respiratory capacity in neonatal mouse ventricular cardiomyocytes (NMVMs) post-DOX treatment (Fig. 3e and Supplementary Fig. 7c). Reduced mitochondrial oxidative phosphorylation (OXPHOS) was associated with abnormal mitochondrial dynamics. Therefore, supplementary experiments were undertaken to evaluate mitochondrial morphology and function in *A. muciniphila*-treated DIC mice. Transmission electron microscopy (TEM) analysis demonstrated that DOX administration led to disordered mitochondrial arrangements, abnormal density, and fragmentation, accompanied by significant cristae disorganization. These detrimental effects were mitigated by *A. muciniphila* treatment (Fig. 3f). Furthermore, DOX-induced mitochondrial fragmentation was ameliorated in *A. muciniphila*-treated mice, as evidenced by improvements in mitochondrial size and area (Fig. 3g, h). In addition, the expression of the mitochondrial fission protein

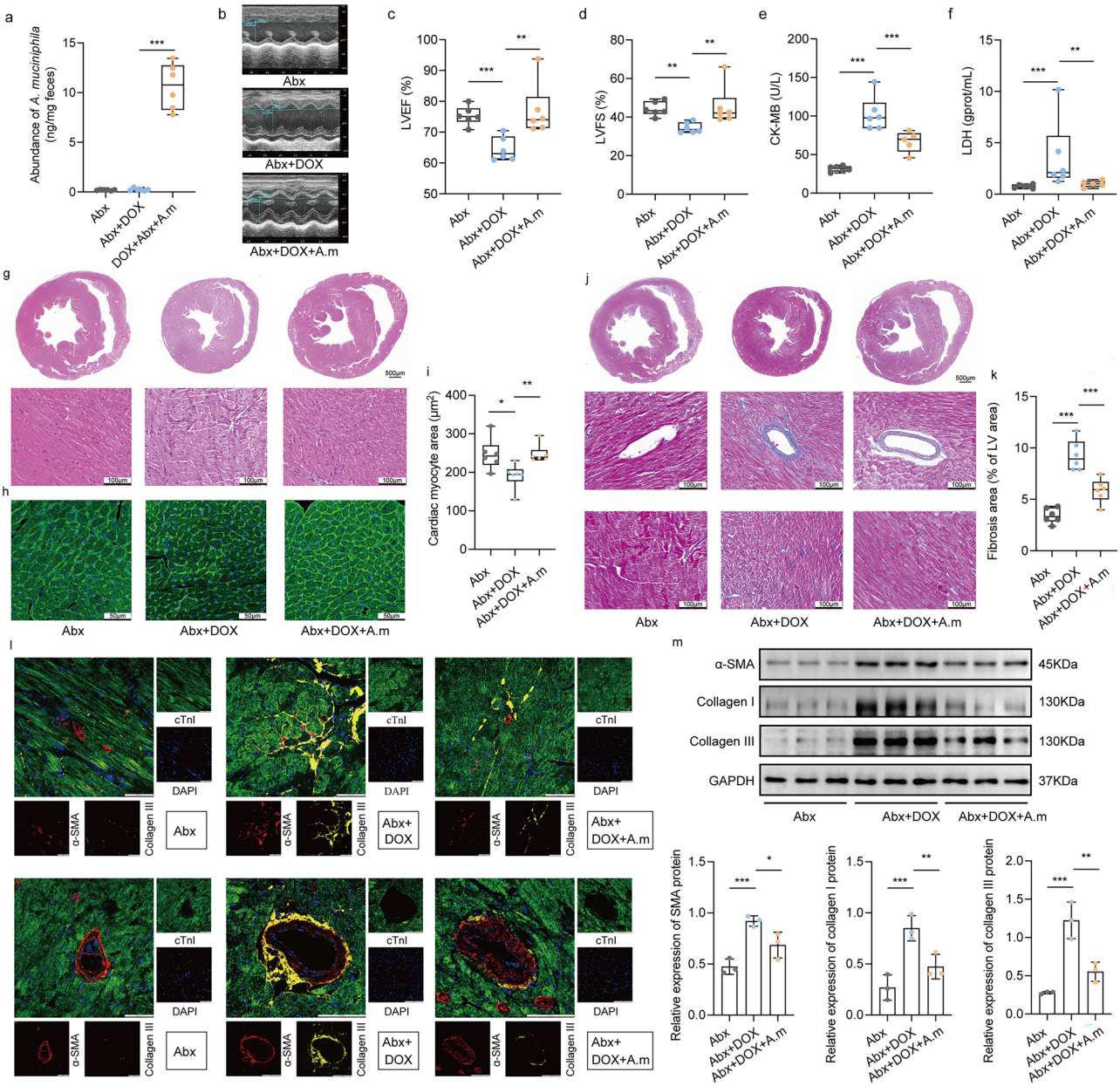

Fig. 2 | *Akkermansia muciniphila* (*A. muciniphila*) colonization alleviates doxorubicin (DOX)-induced cardiomyopathy in antibiotic cocktail (Abx)-treated mice. a Changes in qPCR-based absolute abundances of fecal *A. muciniphila* in mice from indicated group. **b** Anatomic M-mode echocardiography and corresponding electrocardiographic images of hearts from Abx-treated mice, DOX plus Abx-treated mice, and DOX plus *A. muciniphila* and Abx-treated mice ($n = 6$). Changes of echocardiographic **c** left ventricular ejection fraction (LVEF) and **d** left ventricular fraction shortening (LVFS) in the indicated groups ($n = 6$). **e**, **f** Changes of serum lactate dehydrogenase (LDH) and creatine kinase-MB (CK-MB) levels in the three groups ($n = 6$). **g** Representative H&E staining images of the heart tissue section from mice in the indicated groups. Bar = 100 μm ($n = 6$). **h** Wheat germ agglutinin (WGA) staining of myocardial tissue sections to evaluate cardiac atrophy. Bar = 50 μm. **i** Quantitation of myocardial cell size of mice in the indicated groups ($n = 6$). **j** Representative images of myocardial tissue sections stained with Masson's trichrome (from top to bottom, the images are a panoramic view of the heart, a transverse section, and a longitudinal section). **k** Quantification of the fractional area of cardiac fibrosis based on 6 randomly selected fields of stained myocardial tissue sections ($n = 6$). **l** Immunofluorescence staining of heart tissues from indicated groups with cardiac Troponin I (cTnI; green), smooth muscle actin (SMA; red), collagen III (yellow), and DAPI (blue). **m** Western blot analysis and quantification of extracellular matrix-related proteins, smooth muscle actin (SMA), collagen III, and collagen III in DOX-treated mice with or without *A. muciniphila* ($n = 3$). The *P* value was calculated by one-way ANOVA (Dunnett's or Sidak multiple comparisons tests). $^{*}P < 0.05$, $^{**}P < 0.01$, $^{***}P < 0.001$.

dynamin-related protein 1 (DRP1) was upregulated, whereas the fusion protein optic atrophy protein 1 (OPA1) was downregulated in DOX-challenged mouse hearts. This effect was reversed by *A. muciniphila* treatment (Fig. 3i–l). Our results further demonstrated that mitochondrial division was increased in the DOX group, and *A. muciniphila* supernatant reduced the number of mitochondria by inhibiting fission (Supplementary Fig. 8f, g). Collectively, these data indicate that *A. muciniphila* treatment effectively alleviates DOX-induced mitochondrial fragmentation.

A. muciniphila regulates mitochondrial bioenergetics by activating PPARα signaling pathway in DIC mice

Spearman analysis was used to calculate the correlation between the abundance of *A. muciniphila* and DEGs (Supplementary Data 1). We then compared the top 20 *A. muciniphila*-related genes (Supplementary Table 4) with top 20 oxidative phosphorylation-related genes[15], and found 11 overlapped genes as shown in Supplementary Fig. 9a. The heatmap in Fig. 4a showed that TNRC6B, NT5C1A, and PPARα were strongly positively

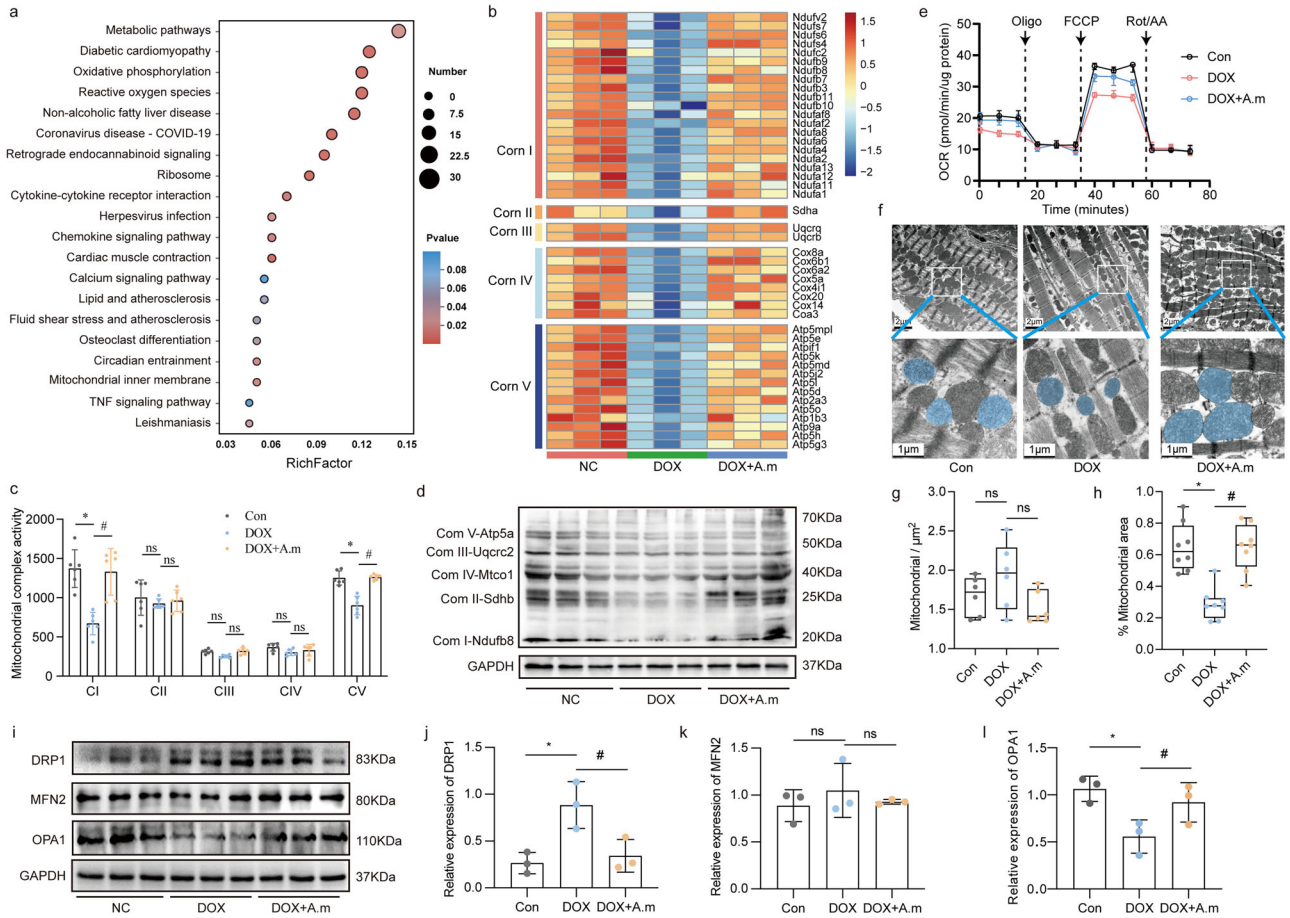

Fig. 3 | Supplement with *Akkermansia muciniphila* (*A. muciniphila*) improves cardiac dysfunction by regulating mitochondrial bioenergetics. a KEGG enrichment analysis of RNA-sequencing data from DOX and control hearts. **b** Heatmap showing differentially expressed mitochondrial respiratory electron transport chain (ETC, Complex I–V) genes in the mouse hearts from indicated groups ($n = 3$). **c** The activity of mitochondrial respiratory chain complexes in the hearts of mice from various groups was assessed using commercial kits ($n = 6$). **d** Representative immunoblotting images and quantification of mitochondrial OXPHOS proteins in mouse heart lysates (antibodies against Ndufb8, Sdhb, Uqcrc2, Mtco1, and Atp5a1 used as representatives for mitochondrial complex I, II, III, IV, and V, and GAPDH used as an internal control, $n = 3$ for each group). **e** Real-time monitoring of the oxygen consumption rate (OCR) in neonatal mouse ventricular cardiomyocytes (NMVMs) with or without DOX/*A. muciniphila* treatment. Data are presented as the mean ± SD ($n = 3$). **f** Representative transmission electron microscopy images of mice hearts from the control, DOX and DOX + *A. muciniphila* group. Scale bar = 2 μm. Quantification of mitochondria-related parameters from (**g**). Mitochondria/μm² refers to the average number of mitochondria ($n = 6$). **h** % mitochondrial area refers to the ratio of mitochondrial area to image area. **i–l** Representative immunoblotting images and quantification of DRP1, MFN2, and OPA1 in the heart tissues from the control, DOX and DOX + *A. muciniphila* group ($n = 3$). Mean ± SD. For statistical analysis, two-way ANOVA with Tukey's test for multiple comparisons was used. ns, no significance; $^{*}P < 0.05$ vs. NC group; $^{\#}P < 0.05$ vs. DOX group.

correlated with *A. muciniphila*, LVEF, and LVFS, but negatively correlated with CM-MB and LDH. PPARα is identified as a regulator of fatty acid oxidation and mitochondrial biogenesis and function[16,17]. The STRING-based protein–protein interaction (PPI) network demonstrated that PPARα was closely related to the oxidative phosphorylation-related proteins (Supplementary Fig. 9b). Additionally, we found that PPARα was closely correlated with ETC complex proteins (Ndufb8, Sdhb, Mtco1, Atp5a, etc.) (Supplementary Fig. 9c). We then confirmed that *A. muciniphila* treatment reversed the DOX-induced decrease in cardiac PPARα and its coactivator peroxisome proliferator-activated receptor gamma coactivator 1-alpha (PGC1α) expression, both at mRNA and protein levels (Fig. 4b–d). The results of immunofluorescence found that PPARα was mostly located in the nucleus and mitochondrion of cardiomyocyte (Fig. 4d). To further validate the role of PPARα signaling pathway in the cardioprotective role of *A. muciniphila* on DIC mice, we used PPARα-specific antagonist NXT629 to block the biological function of PPARα signaling (Fig. 4f)[18]. As expected, NXT629 decreases DOX-induced cardiac fibrosis and decreases the protective effects of *A. muciniphila* as revealed by echocardiography, H&E, and Masson trichrome staining (Fig. 4f–j). In addition, the regulation of imbalanced mitochondrial fusion by *A. muciniphila* was counteracted with inhibition of PPARα signaling pathway (Fig. 4k). In vitro, the improvement of *A. muciniphila* supernatant on DOX-induced cell toxicity was abolished by the addition of NXT629 (Supplementary Fig. 10a). In addition, NXT629 abrogated the effects of 8% *A. muciniphila* supernatant on ATP level and JC-1 ratio caused by DOX treatment (Supplementary Fig. 10b–d). Furthermore, DOX-induced the division of mitochondria was alleviated by the supernatant of *A. muciniphila*, but further reversed with the addition of NXT629 (Supplementary Fig. 10e, f). These results showed that PPARα/PGC1α signaling pathway participated in the cardioprotective effects of *A. muciniphila* and activation of myocyte PPARα may restore mitochondrial bioenergetics and improve DIC.

A. muciniphila supplementation restores the disordered gut microbiota caused by DOX

Metabolites secreted or modified by the microbiota or host mediate host–microbiota interactions[19]. Therefore, 16S rRNA gene sequencing and untargeted metabolomics were used to determine structural changes in gut microbiota and metabolites of DIC mice in response to *A. muciniphila*

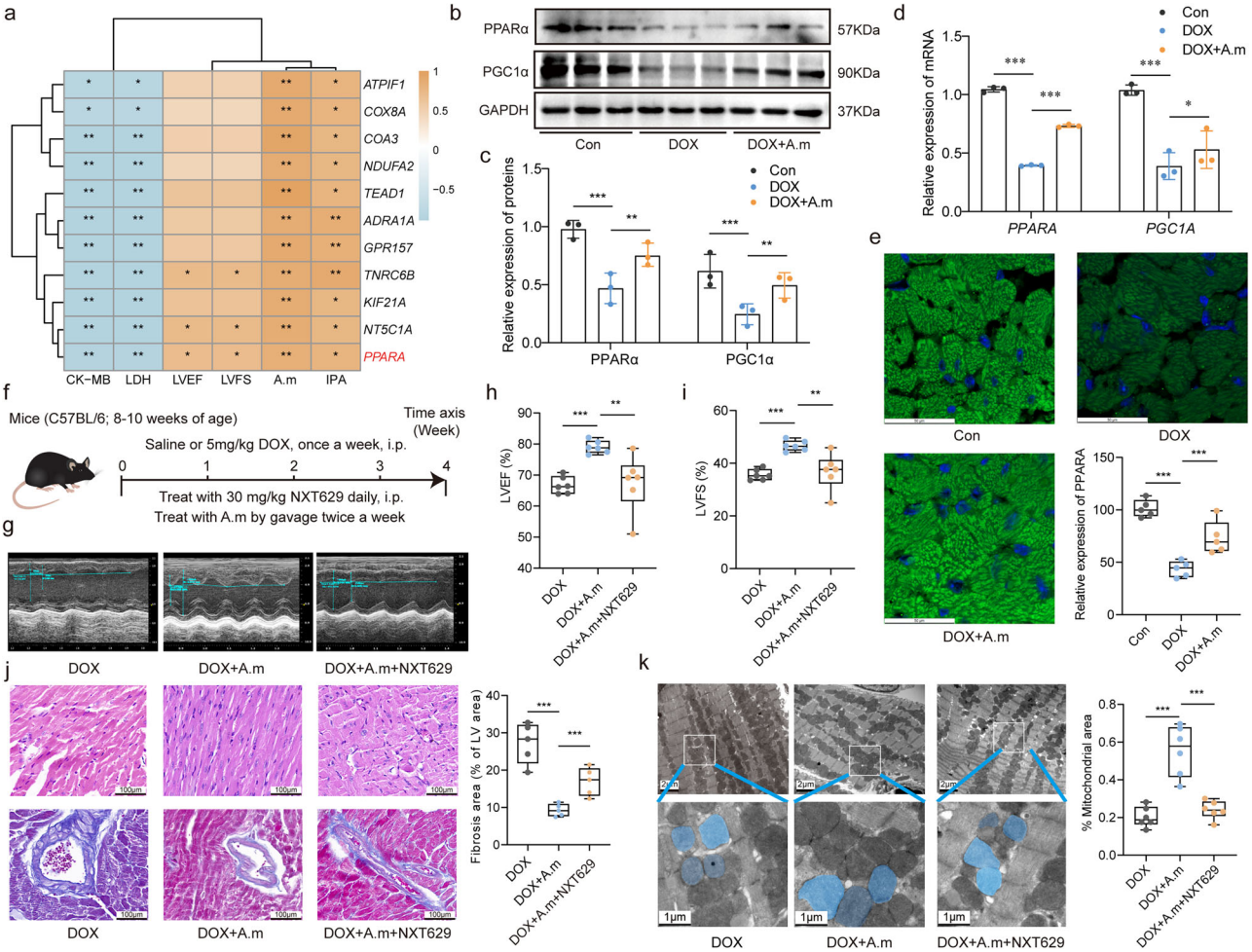

Fig. 4 | *Akkermansia muciniphila* (*A. muciniphila*) administration regulates mitochondrial bioenergetics by activating PPARα/PGC1α signaling pathway. **a** Pearson correlation analysis between the 11 mitochondrial OXPHOS-related genes and *A. muciniphila* levels, as well as cardiac injury markers in mice ($n = 3$). **b**, **c** Representative immunoblotting images and quantification of PPARα and PGC1α in the heart tissues from the control, DOX, and DOX + *A. muciniphila* groups ($n = 3$). **d** RT-qPCR was used to measure the mRNA levels of PPARA and PGC1α, from the heart tissues in the indicated groups ($n = 3$). **e** Immunofluorescence staining of heart tissues from the indicated groups with cardiac PPARα (green) DAPI (blue), as well as semi-quantitative analysis of PPAR fluorescence. **f** Schematic representation of treatment with DOX, *A. muciniphila*, or PPARα inhibitor NXT629 (30 mg/kg). **g** Anatomic M-mode echocardiography and corresponding electrocardiographic images of hearts from DOX, DOX + *A. muciniphila*, and DOX + *A. muciniphila* + NXT629 ($n = 6$). Changes of echocardiographic **h** left ventricular ejection fraction (LVEF) and **i** left ventricular fraction shortening (LVFS) in the indicated groups ($n = 6$). **j** Representative images of myocardial tissue sections stained with Masson's trichrome (from top to bottom, a transverse section and a longitudinal section). Quantification of the fractional area of cardiac fibrosis based on 6 randomly selected fields of stained myocardial tissue sections ($n = 6$). **k** Representative transmission electron microscopy images of mice hearts from the three group. Scale bar = 2 μm. % mitochondrial area refers to the ratio of mitochondrial area to image area ($n = 6$). Data presented as mean ± SD. For statistical analysis, two-way ANOVA with Tukey's test for multiple comparisons was used. $^{*}P < 0.05$, $^{**}P < 0.01$, $^{***}P < 0.001$.

treatment. As shown in Fig. 5a, α diversity of the microbiome in the control, DOX, and DOX_ *A. muciniphila* groups, presented with Chao1, observed reads, Coverage, Shannon_2, and Simpson, remained at a similar level. The results of PCoA analysis revealed that mice in the DOX group were different from other groups, which indicated that *A. muciniphila* distinctly changed β diversity of DIC mice (Fig. 5b). At the phylum level, we found that Firmicutes, Verrucomicrobia and Bacteroidetes accounted for more than 95.0% of the whole gut microbial composition in three groups. Firmicutes was more abundant in DIC mice compared with the control group and was decreased by *A. muciniphila* supplementation. In contrast, the abundance of Verrucomicrobia was decreased in the DOX group; while its relative abundance was increased in the DOX_ *A. muciniphila* group (Supplementary Fig. 11a, b). Notably, *A. muciniphila* colonization significantly altered the bacterial structure at the genus level by contributing to the abundance of *A. muciniphila* populations and reducing the abundance of Lactobacillus (Fig. 5c). To infer the differential taxonomic markers in *A. muciniphila*-treated mice, LEfSe was used. The results revealed that at genus level, *A. muciniphila*, *Ruminococcaceae_UCG*, *Acetitomaculum*, *Ruminococcus_2*, and *Lachnospiraceae_NK4B4* were enriched in the control group, whereas *Lactobacillus*, *Reyranella*, *Alistipes*, *Rikenellaceae_RC9*, and *Rikenella* were enriched in the DOX group. In addition, *Turicibacter*, *Escherichia*, *Candidatus_Megaira*, *Desulfovibrio*, *Oleiphilus*, and *Opitutus* were enriched in the DOX + *A. muciniphila* group (Fig. 5d and Supplementary Fig. 11c). The ternary plots reveal significant alterations in the gut microbiota of DIC mice compared to the control group. Furthermore, the gut microbiota composition exhibits distinct differences between the DOX and DOX_ *A. muciniphila* groups (Fig. 5e). A Spearman correlation analysis was performed to evaluate the potential association between alterations in gut microbiota composition and parameters of cardiac injury. The genus *A. muciniphila* was positively correlated with LVEF and LVFS, but negatively correlated with plasma LDH and CK-MB. Additionally, *Rikenellaceae_RC9_gut_group*, *Alistipes*, *Helicobacter*, and *Rikenella* were negatively correlated with LVEF and LVFS, but positively correlated with plasma LDH and CK-MB (Supplementary Fig. 11d). The integrity of the intestinal barrier

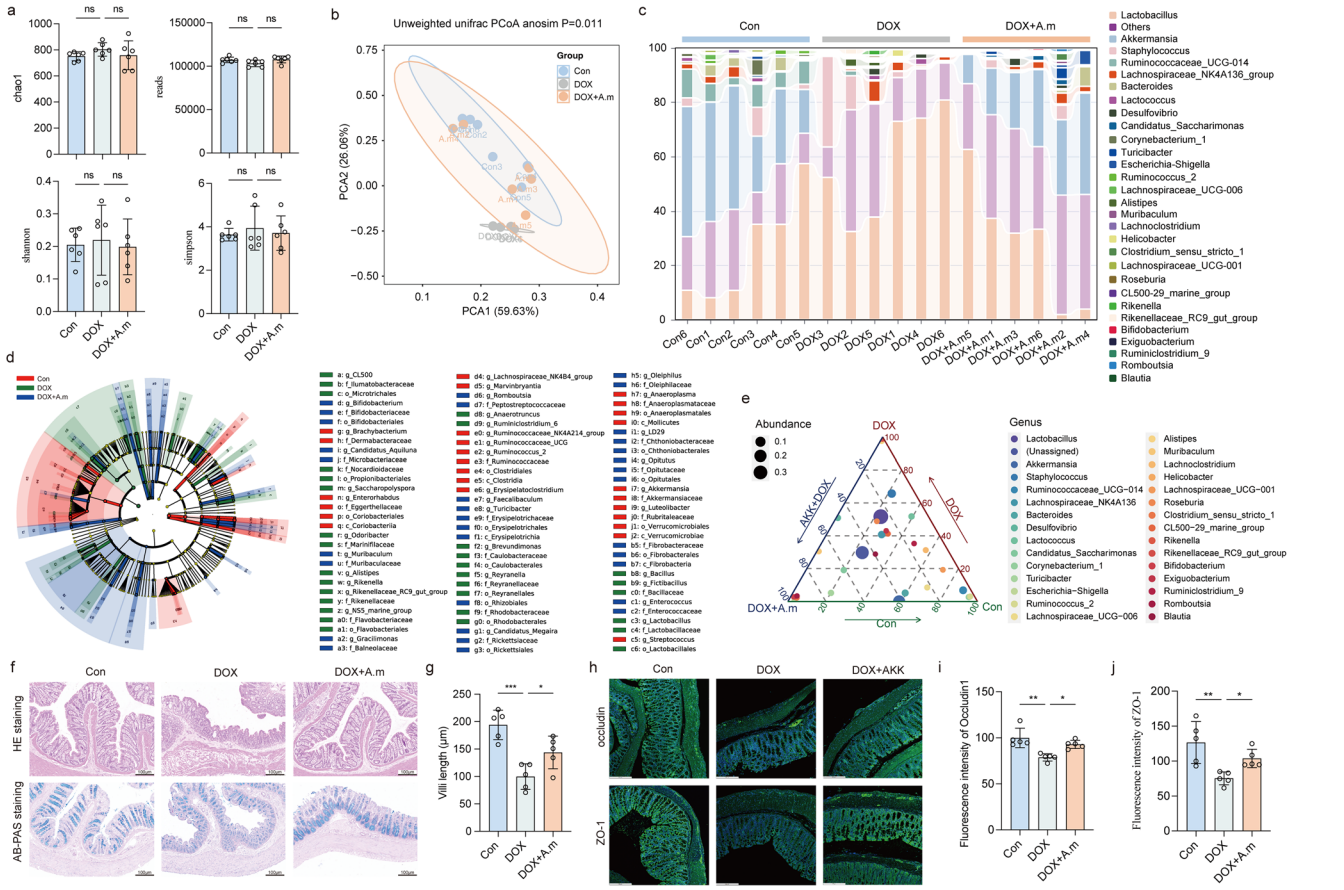

Fig. 5 | Fecal microbiome analysis of *Akkermansia muciniphila* (*A. muciniphila*)-treated mice under doxorubicin (DOX) stimulation. a Boxplots of a-diversity calculated by Chao, Shannon_2, Simpson, and observed reads ($n = 4$). **b** PCoA plot based on unweighted Unifrac distance was used to test the variations of microbial communities among groups ($n = 4$). **c** Relative abundance of differential genera in the three groups were illustrated ($n = 4$ per group). **d** Statistical differences among the control, DOX, and DOX + *A. muciniphila* groups were identified using the linear discriminant analysis (LDA) effect size (LEfSe) method. Cladogram illustrating the output of the LEfSe algorithm. Significantly distinct taxonomic nodes are colored, and the branch areas are shaded according to the effect size of the taxa ($n = 4$). **e** Ternary plots reveal OTUs relative abundance (dot size) at the genus level among the three sample groups. Generalist taxa are represented as circles in the middle of the triangle, sample-specific bacterial taxa are represented as circles in the summit or along the edges of the triangle ($n = 4$). **f** Representative hematoxylin and eosin (H&E) staining and periodic acid Schiff (PAS) staining of the ileum. Scale bar: 100 μm. **g** The villi length of the ileum was measured ($n = 6$). **h–j** Immunofluorescence staining of ileum tissues from indicated groups with occluding and ZO-1, as well as semi-quantitative analysis of protein fluorescence ($n = 3$). Data presented as mean ± SD. For statistical analysis, two-way ANOVA with Tukey's test for multiple comparisons was used. $^{*}P < 0.05$, $^{**}P < 0.01$, $^{***}P < 0.001$.

plays a vital role in the interaction between gut microbiota and gastrointestinal metabolites[19]. Our findings indicate that the ileal villi in DIC mice exhibited flattening and a reduction in length; however, this alteration was mitigated by treatment with *A. muciniphila* (Fig. 5f, g). The colonization of *A. muciniphila* to DIC mice also elevated several ileal tight-junction proteins (occludin1 and ZO-1) that were decreased in DIC mice, as evidenced by immunofluorescence (Fig. 5h–j) and Western blot analysis (Supplementary Fig. 12a–c). The *A. muciniphila* colonization also elevated gene expression levels of the ileal tight junction that were decreased in DIC mice, including *ZO1*, occludin (Ocln), claudin (Cldn) 1, and Cldn3 (Supplementary Fig. 12d–h). Therefore, the findings suggest that the administration of *A. muciniphila* may confer protective effects against DOX-induced intestinal barrier damage and gut microbiota dysbiosis.

Reduced IPA is linked to the depletion of *A. muciniphila*

We conducted untargeted metabolite profiling on both fecal samples (Supplementary Data 2) and serum samples (Supplementary Data 3) from the control, DOX, and DOX_*A. muciniphila* groups. Principal component analysis (PCA) results indicated significant separation among all groups, suggesting a high degree of differentiation (Fig. 6a, b). The administration of *A. muciniphila* to DIC mice elevated 105 fecal metabolites (Supplementary Fig. 13a, b). In addition, *A. muciniphila* elevated 133 serum metabolites (Supplementary Fig. 13c, d). The top 100 changed fecal and serum metabolites were illustrated in Supplementary Fig. 13e, f. We analyzed the interactions between gut microbiota, fecal and serum metabolites, and transcriptome data to understand *A. muciniphila*'s effect on mitochondrial bioenergetics in DIC mice. Spearman's rank correlations were calculated for the top 10 differentially expressed genera, 30 fecal metabolites, 30 serum metabolites, and 30 DEGs to identify key metabolites involved in *A. muciniphila* 's mitigation of cardiotoxicity in mice. Changes in the abundances of Lactobacillus, Bacteroides, and Lachnospiraceae UCG-006 induced by the *A. muciniphila* administration were closely associated with alterations in various fecal metabolites (L-arogenate, pentadecanoic acid) and serum metabolites (taurine, creatinine, and palmitoyl sphingomyelin), subsequently related to modulation of cardiac function (Supplementary Fig. 14). The predictive pathway enrichment was performed using differential serum metabolites among the three groups. The metabolites illustrated Phenylalanine, tyrosine and tryptophan biosynthesis, taurine and hypotaurine metabolism, tryptophan metabolism, etc. (Fig. 6c). Several studies reported that *A. muciniphila* may be associated with altered tryptophan metabolism[20,21] and similarly, the results of Fig. 6d showed that *A. muciniphila* reversed the altered abundance of tryptophan metabolites in DIC mice including tryptophan (Trp), indole-3-pyruvate (IPyA), indole-3-lactic acid (ILA), IPA, indole-3-acetamide (IAM), indole acetic acid (IAA) and indole-

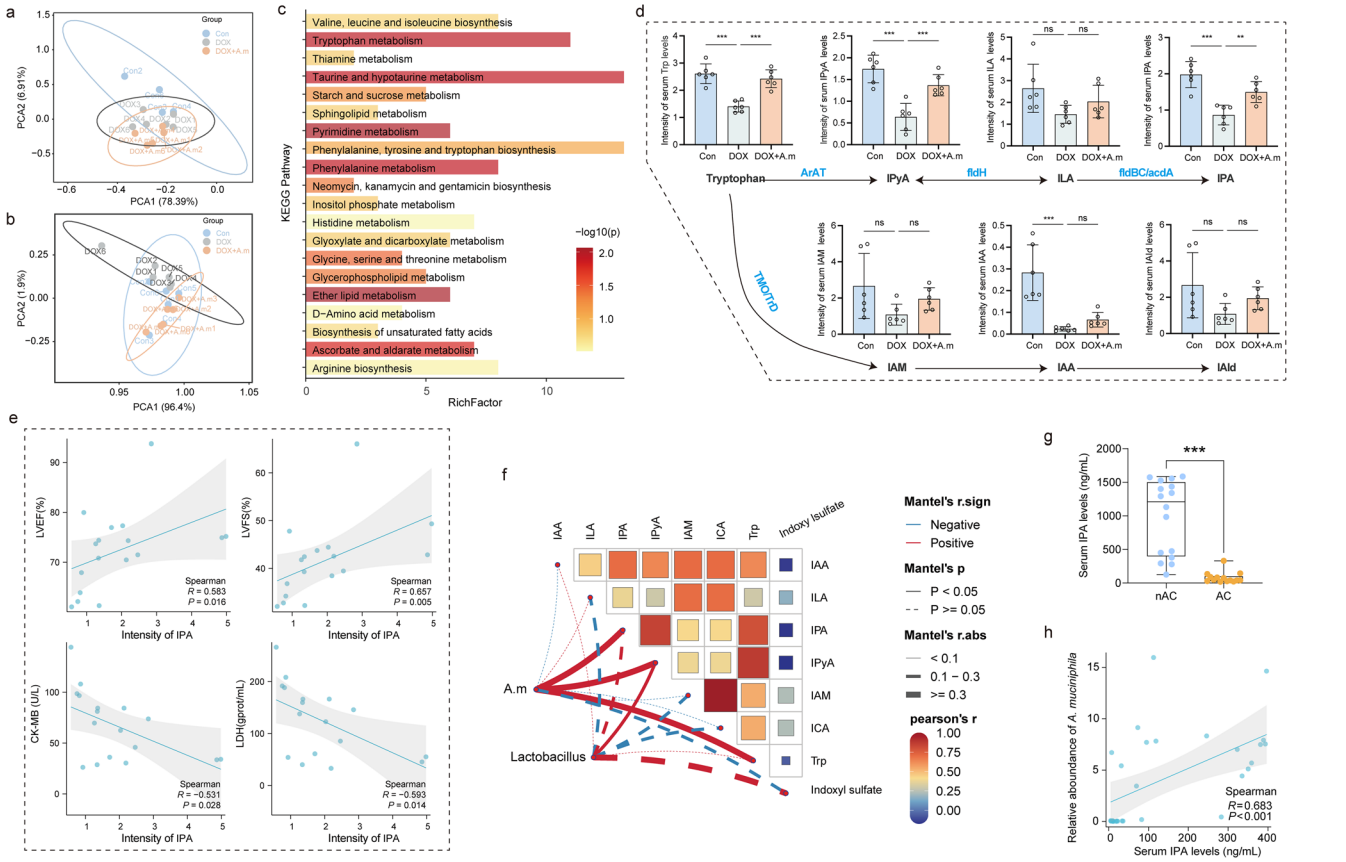

Fig. 6 | *Akkermansia muciniphila* (*A. muciniphila*) modulates the microbial tryptophan metabolites profile of doxorubicin (DOX)-treated mice. Principal component analysis of **a** fecal metabolites and **b** serum metabolites among the control, DOX, and DOX + AKK groups ($n = 6$). **c** Bar chart of significantly different KEGG metabolic pathways (based on serum metabolites) among the control, DOX, and DOX + AKK groups ($n = 6$). **d** Serum concentrations of metabolites in tryptophan metabolism (ArAT aromatic amino acid aminotransferase, IPyA indole-3-pyruvate, fldH phenyllactate dehydrogenase, ILA indole-3-lactic acid, fldBC phenyllactate dehydratase, acdA acyl-Coa dehydrogenase, IPA indole-3-propionic acid, TMO tryptophan 2-monooxygenase, TrD tryptophan decarboxylase, IAM indole-3-acetamide, IAA indole acetic acid, IAId indole-3-aldehyde) among three groups of mice ($n = 6$). **e** Spearman correlation analysis between the IPA levels and cardiac injury markers (LVEF left ventricular ejection fraction, LVFS left ventricular fraction shortening, LDH lactate dehydrogenase, CK-MB creatine kinase-MB) in mice from the three groups ($n = 18$). **f** Pairwise comparisons of tryptophan metabolites, with a color gradient denoting Spearman's correlation coefficient. The correlation between the bacterial expression profiles and each metabolite was determined using partial Mantel tests. The edge width corresponds to Mantel's R statistic for the corresponding distance correlations, and the edge color denotes statistical significance ($n = 6$). **g** Serum levels of IPA in all participants (anthracycline, AC: $n = 14$; non-anthracycline, nAC: $n = 16$). **h** Spearman correlation analysis between the serum IPA levels and relative abundance of *A. muciniphila* in all participants. Data presented as mean ± SD. For statistical analysis, two-way ANOVA with Tukey's test for multiple comparisons was used. $^{**}P < 0.01$, $^{***}P < 0.001$.

3-aldehyde (IAId). IPA was positively correlated with LVEF and LVFS, but negatively correlated with CK-MB and LDH (Fig. 6e). We further carried out liquid chromatography mass spectrometry to identify the component of *A. muciniphila* supernatant. Interestingly, compared with the blank culture medium, oxindole was decreased, while ILA, IPA, and indole-3-glycol aldehyde were increased in the supernatant of *A. muciniphila*, indicating that *A. muciniphila* was able to produce IPA directly. Except ILA, serum indole-3-glycol aldehyde, and oxindole showed no significant correlation with LVEF in mice (Supplementary Fig. 15). Subsequently, we analyzed the association among serum tryptophan metabolites, *A. muciniphila* and Lactobacillus, which accounted for more than 50.0% of the identified gut microbial composition in Fig. 5c. Combining microbiota with that of metabolomes showed that *A. muciniphila* was strongly and positively correlated with serum Trp, IPyA, and IPA, while Lactobacillus showed no significantly correlated with any tryptophan metabolites (Fig. 6f). That is to say, gut microbiota and tryptophan metabolites indeed mediate the cardioprotective role of *A. muciniphila* to DIC. Among these tryptophan metabolites, IPA was shown to protect the heart from oxidative stress[10,22], and act as a new biomarker for heart failure[23]. We therefore measured the serum levels of IPA in our cohorts and found IPA was significantly decreased in the AC group compared to the nAC group (989.1 vs. 79.97 ng/mL, $P < 0.001$, Fig. 6g). Moreover, IPA was positively correlated with *A. muciniphila* (Fig. 6h). Collectively, these findings indicated that IPA is a crucial metabolite through which *A. muciniphila* exerts its cardioprotective effects against DIC.

IPA attenuates DIC by regulating mitochondrial bioenergetics

The addition of IPA in a chow diet is approved to improve heart failure with preserved ejection fraction in mice[22]. Therefore, DIC mice were gavage with low (20 mg/kg/day) and high (40 mg/kg/day) concentration of IPA for continuous 4 weeks (Fig. 7a). In line with our hypothesis, IPA reversed the reduction of cardiac function and elevation of cardiac injury markers induced by DOX (Fig. 7b–f). Accordingly, IPA alleviated DOX-induced myocardial injury, atrophy and fibrosis (Fig. 7g, h). Consistently, the addition of both low and high concentrations of IPA reversed the increase in SMA and collagen III protein levels caused by DOX (Fig. 7i–l). We further investigate whether IPA protects against DIC by regulating DOX-induced mitochondrial dysfunction. Interestingly, IPA was found to restore the mitochondrial bioenergetics disrupted by DOX, indicated by increased mitochondrial area (Fig. 8a–c), improved mitochondrial respiratory chain complex I and V (Fig. 8d), and increased ETC complex expression (Fig. 8e) compared with DOX-treated hearts. IPA also reversed DOX-induced excessive mitochondrial fragmentation, with decreased levels of DRP1 and

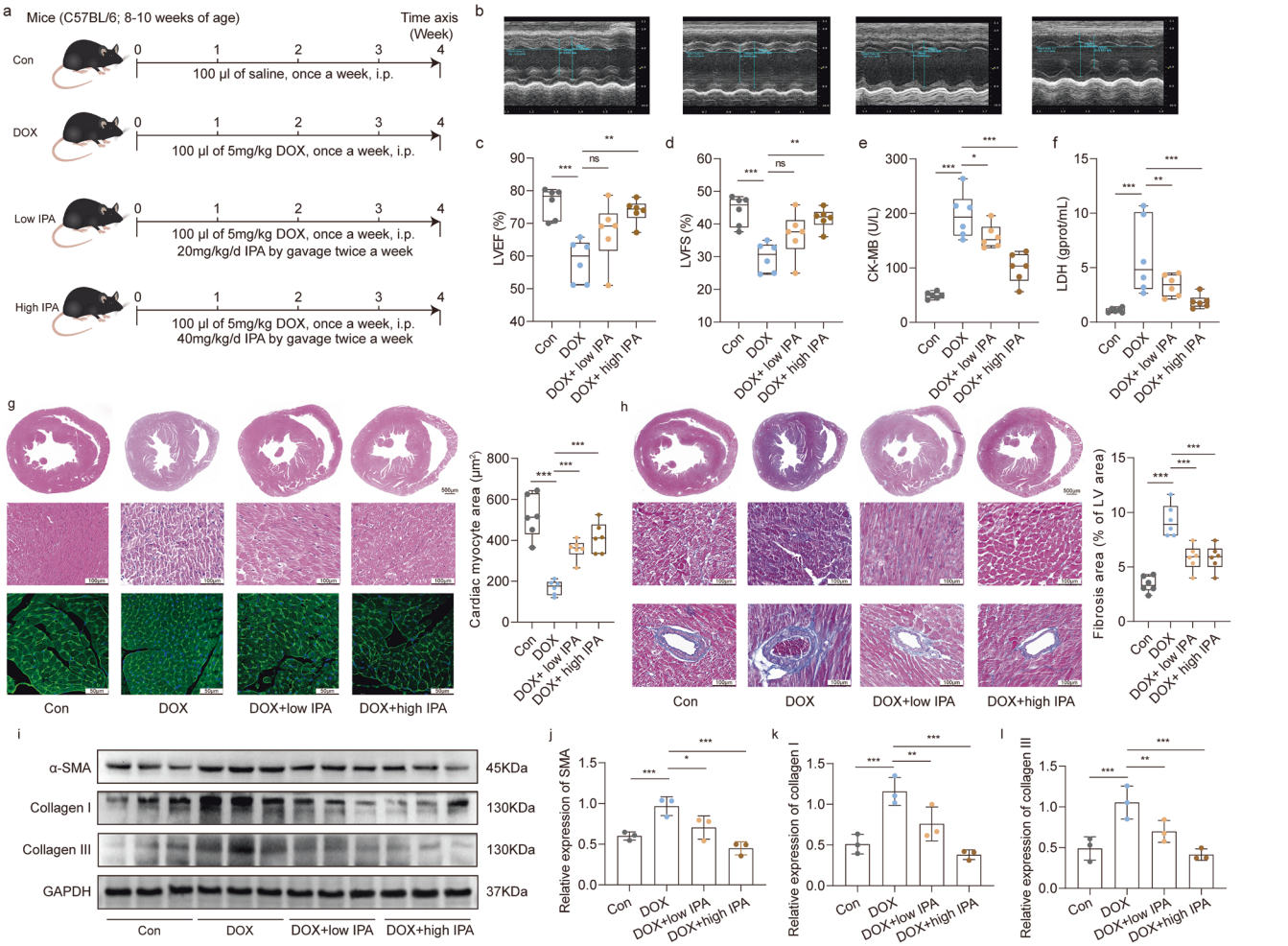

Fig. 7 | Indole-3-propionic acid (IPA) supplementation alleviates doxorubicin (DOX)-induced cardiac dysfunction, atrophy, and fibrosis in C57BL/6 mice. **a** Schematic representation of treatment with doxorubicin (DOX) and low IPA (20 mg/kg) or high IPA (40 mg/kg) ($n = 6$ per group). **b** Anatomic M-mode echocardiography and corresponding electrocardiographic images of hearts from the indicated groups ($n = 6$). Changes of echocardiographic **c** left ventricular ejection fraction (LVEF) and **d** left ventricular fraction shortening (LVFS) in the indicated groups ($n = 6$). **e**, **f** Changes of serum lactate dehydrogenase (LDH) and creatine kinase-MB (CK-MB) levels in the four groups ($n = 6$). **g** Upper panel: representative H&E staining images of the heart tissue section from mice in the indicated groups. Bar = 100 μm. Bottom panel: wheat germ agglutinin (WGA) staining of myocardial tissue sections to evaluate cardiac atrophy. Bar = 50 μm. Right panel: quantitation of myocardial cell size of DIC mice in the indicated groups ($n = 6$). **h** Representative ×200 images of myocardial tissue sections stained with Masson's trichrome (from top to bottom, the images are a panoramic view of the heart, a transverse section, and a longitudinal section). Right panel: quantification of the fractional area of cardiac fibrosis based on 6 randomly selected fields of stained myocardial tissue sections ($n = 6$). **i–l** Western blot analysis and quantification of extracellular matrix-related proteins, smooth muscle actin (SMA), collagen III, and collagen III in DOX-treated mice with IPA ($n = 3$). Data presented as mean ± SD. For statistical analysis, two-way ANOVA with Tukey's test for multiple comparisons was used. $^{*}P < 0.05$, $^{**}P < 0.01$, $^{***}P < 0.001$.

increased OPA1 protein (Fig. 8f). In vitro, IPA above 250 μM produces significant toxicity to H9C2 cells (Supplementary Fig. 16a), whereas IPA within 100 μM notably improve the toxicity of myocardial cells induced by DOX (Supplementary Fig. 16b). Notably, both 50 and 100 μM of IPA increased the production of ATP in DOX-treated H9C2 cells (Supplementary Fig. 16c). The results of JC-1 staining revealed that IPA improved DOX-induced reduction of mitochondrial membrane potential (Supplementary Fig. 16d, e). DOX-induced the division of mitochondria was alleviated by the IPA administration (Supplementary Fig. 16e, f). Moreover, IPA treatment effectively restored mitochondrial respiratory capacity in NMVMs cells after DOX treatment (Fig. 8g–k). Thus, IPA protected against DOX-induced mitochondrial dysfunction and cardiotoxicity.

IPA binds AhR to activate PPARα signaling pathway, exerting its anti-cardiotoxicity effects

As *A. muciniphila* may alleviate DIC by activating PPARα signaling pathway (Fig. 4), we performed additional experiments to validate whether IPA improved DOX-induced mitochondria dysfunction via PPARα pathway and its potential mechanism. As shown in Supplementary Fig. 17a–c, both low and high IPA increased cardiac PPARα and PGC1α protein levels in DOX-treated mice. In vitro, 8% *A. muciniphila* supernatant or IPA alone upregulated PPARα and PGC1α mRNA in NMVMs after a 24 h exposure (Supplementary Fig. 17d, e), indicating that IPA increases PPARα at the transcript level. Previous studies have found that IPA exerts its function by binding pregnane X receptor[24] and AhR[25]. Because pregnane X receptor was not detected in the heart[22], we sought to investigate whether IPA activates PPARα by binding AhR. Our results confirmed that IPA increased AhR protein expression in the heart (Supplementary Fig. 17f, g). We observed a significant increase in nuclear AhR protein levels and a decrease in cytosolic AhR protein levels following IPA treatment (Supplementary Fig. 17h–j). Consistently, subsequent immunofluorescence showed that AhR, which was co-localized with PPARα, was primarily expressed in the cytoplasm in NMVMs; DOX treatment decreased fluorescence intensity of PPARα, while IPA treatment caused AhR to translocate into the nucleus and increased fluorescence intensity of PPARα (Supplementary Fig. 17k). We investigated whether AhR acts as a transcription factor to promote PPARα expression.

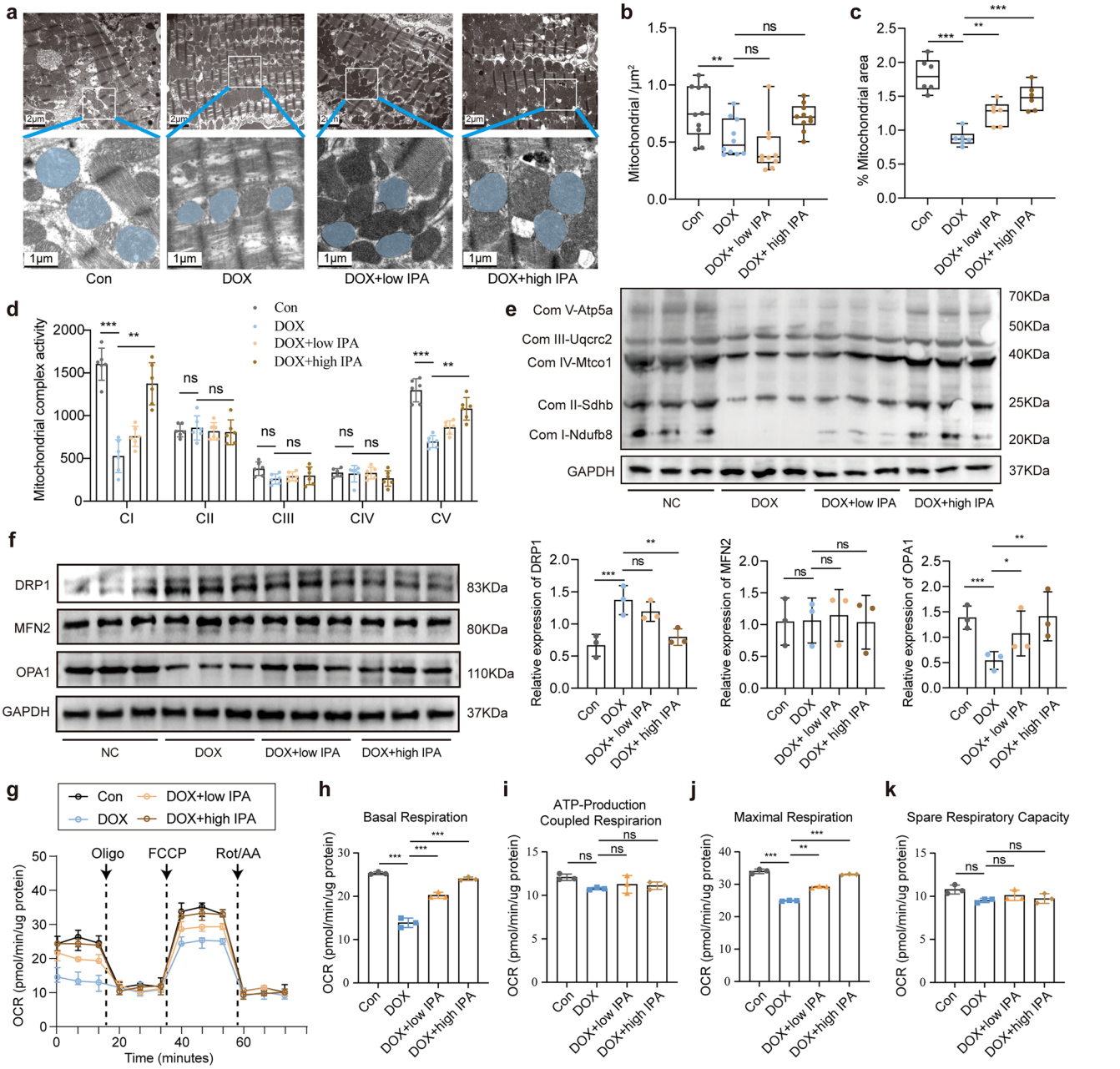

Fig. 8 | Indole-3-propionic acid (IPA) administration improves doxorubicin (DOX)-induced mitochondrial dysfunction. a Representative transmission electron microscopy images of mice hearts from the control, DOX, and DOX + IPA group. Scale bar = 2 μm. Quantification of mitochondria-related parameters from (**b**). Mitochondria/μm^2 refers to the average number of mitochondria ($n = 6$). **c** % mitochondrial area refers to the ratio of mitochondrial area to image area ($n = 6$). **d** The activity of mitochondrial respiratory chain complexes in the hearts of mice from various groups was assessed using commercial kits ($n = 6$). **e** Representative immunoblotting images and quantification of mitochondrial OXPHOS proteins in mouse heart lysates (antibodies against Ndufb8, Sdhb, Uqcrc2, Mtco1, and Atp5a1 used as representatives for mitochondrial complex I, II, III, IV, and V, and GAPDH used as an internal control, $n = 3$ for each group). **f** Representative immunoblotting images and quantification of DRP1, MFN2 and OPA1 in the heart tissues from the control, DOX, and DOX + IPA groups ($n = 3$). **g**–**k** Real-time monitoring of the oxygen consumption rate (OCR) in neonatal mouse ventricular cardiomyocytes (NMVMs) with or without DOX/IPA treatment. Data are presented as the mean ± SD ($n = 3$). Mean ± SD. For statistical analysis, two-way ANOVA with Tukey's test for multiple comparisons was used. *$P < 0.05$, **$P < 0.01$, ***$P < 0.001$.

Using the AhR antagonist GNF35125[26] on H9C2 cells, we found that GNF351 inhibited the IPA-induced upregulation of PPARα and PGC1α, but not AhR (Supplementary Fig. 18a, b). This confirms that IPA enhances PPARα expression via AhR binding. Notably, GNF351 reduces the protective effect of IPA on cardiomyocytes (Supplementary Fig. 18c), leading to decreased ATP levels (Supplementary Fig. 18d), reduced mitochondrial membrane potential (Supplementary Fig. 18e, f), and increased mitochondrial fission (Supplementary Fig. 18g, h). To validate that IPA's cardioprotective effects are AhR-dependent in vivo, shAhR was delivered via intravenous AAV9-cTnT-shAhR to achieve cardiac-specific AhR knockdown. Successful infection was confirmed by EGFP fluorescence and reduced AhR expression in cardiomyocytes (Supplementary Fig. 19a). The AAV9-sh-AhR group showed reduced AhR expression (Supplementary Fig. 19b, c). AhR knockdown prevented the IPA-induced rise in PPARα and PGC1α protein levels (Supplementary Fig. 19d–g). AhR knockdown impaired IPA's cardioprotective effects in DOX-induced heart dysfunction (Supplementary Fig. 17l–n). In addition, it blocked IPA's benefits on myocardial fiber disorder, fibrosis, and atrophy (Supplementary Fig. 17o–r).

These results indicate that IPA binds to cardiac AhR, activating the PPARα/PGC1α pathway to exert anti-cardiotoxic effects.

Discussion

In this study, the progression of DIC was tracked by observing shifts in the fecal microbial composition of mice. Notably, *A. muciniphila* abundance nearly vanished within the first week of DOX administration and remained low through the fourth week. This trend was also observed in breast cancer patients undergoing DOX therapy. *A. muciniphila* is a Gram-negative, strictly anaerobic bacterium within the phylum Verrucomicrobiota. It utilizes host-derived mucins as a nutrient source and is predominantly present in the intestines of healthy individuals[27]. Recent research has indicated that *A. muciniphila* is correlated with various metabolic diseases, including obesity, diabetes, and inflammatory bowel disease[28]. *A. muciniphila* has been linked to the enhancement of intestinal barrier function, reduction of intestinal inflammation, and promotion of gut health, suggesting its significant role in maintaining intestinal health and regulating metabolic processes[29]. *A. muciniphila* also plays a crucial role in cardiovascular disease. Its abundance is nearly depleted in the intestines of patients or mice with abdominal aortic aneurysms[30]. Reduced *A. muciniphila* levels have been identified as an independent risk factor for cold-related atrial fibrillation in humans[31], Moreover, Supplementation with *A. muciniphila* reversed the exacerbation of atherosclerotic lesions induced by a Western diet by restoring the gut barrier[32]. Although the role of *A. muciniphila* in cardiovascular disease has been somewhat validated, research on its effects in cardiomyopathy is limited. Only one recent study has shown that *A. muciniphila* colonization can reduce the burden on adult worms and muscle larvae while also alleviating the severity of cardiac fibrosis induced by *T. spiralis*[33]. We, for the first time, observed that *A. muciniphila* administration effectively improved mitochondrial function and alleviated DIC.

Another new finding regarding the mechanism by which *A. muciniphila* alleviates DIC is the activation of the PPARα/PGC1α signaling pathway. RNA sequencing identified that PPARα plays a crucial role in the anti-cardiotoxicity ability of *A. muciniphila* on DIC. Mitochondria are the key target for DIC. DOX interrupted mitochondrial OXPHOS, resulting in abnormal mitochondrial bioenergetics, mitochondria dysfunction and cardiomyocytes apoptosis[34]. The PPAR family consists of PPAR-α, PPARγ, and PPARβ, with their expression varying across different tissues. Among them, PPAR-α is most abundantly expressed in the heart[35]. PPAR-α can bind directly to specific PPAR-α response elements, regulating gene expression, and plays a crucial role in managing oxidative stress[36]. The reduced expression of PPARα is linked to the severity of non-alcoholic fatty liver disease[37]. In this study, we found that DOX treatment led to decreased cardiac PPARα/PGC1α signaling pathway, which was restored with *A. muciniphila* administration. Activation of PPARα/PGC1α pathway has therapeutic effects on heart failure[38,39]. However, when PPARα was inhibited by its antagonist NXT629, the protective effects of *A. muciniphila* on DOX-induced mitochondrial dysfunction were lost. These findings suggest that *A. muciniphila* modulates mitochondrial bioenergetics by activating the PPARα signaling pathway in DIC mice.

Probiotic treatment often provides organ protection by producing specific gut metabolites that act through the circulatory system, specifically via the gut–brain axis[40] and gut–heart axis[41]. Research has established the association between *A. muciniphila* tryptophan metabolism. *A. muciniphila* colonization can enhance tryptophan metabolism, leading to increased 5-hydroxytryptamine and decreased kynurenine levels, which in turn alleviates depressive or anxiety in mice[42,43]. *A. muciniphila* is positively correlated with the activity of the epithelial tryptophan-metabolizing enzyme indoleamine 2,3-dioxygenase 1 (IDO1), which enhances the expression of markers associated with stem cells, goblet cells and tuft cells through its interaction with the AhR[44]. Through a comprehensive analysis of the microbiome and metabolome characteristics following *A. muciniphila* intervention, we confirmed tryptophan metabolism as the most probable metabolic pathway by which *A. muciniphila* influences DIC. However, DOX does not impact the serotonin or kynurenine pathways in tryptophan metabolism[45], but significantly reduces the levels of various indole metabolites within the indole/AhR pathway. Among these indole derivatives, IPA was found to be significantly associated with cardiac injury and may act as a mediator connecting *A. muciniphila* and cardiac mitochondria.

Our prior research showed that FMT alleviates DIC by modulating the balance of cardiac mitochondrial fission and fusion and subsequent correlation analysis identified IPA as a key mediator through which FMT link to the heart mitochondria[10]. IPA represents known ligands of the immunomodulatory transcription factor AhR[46]. IPA is decreased in both heart tissue and circulation in mice following a high-fat diet, and dietary supplementation with IPA protects against diastolic dysfunction in heart failure with preserved ejection fraction by enhancing the nicotinamide adenine dinucleotide salvage pathway[22]. In this study, using 16S rRNA sequencing and metabolomic analysis, we examined the changes in serum metabolites in DIC mice following colonization by *A. muciniphila*, along with direct metabolite detection in *A. muciniphila* culture supernatants via liquid chromatography-mass spectrometry (LC-MS). We elucidated the biological role of *A. muciniphila* in producing IPA and mitigating DOX-induced mitochondrial toxicity in cardiomyocytes. However, we did not quantify the serum IPA concentration-time profile following oral IPA administration. To advance clinical translation, further investigations are required to establish the dose-response relationship between *A. muciniphila* and IPA, as well as to characterize IPA's oral bioavailability, pharmacokinetics, and tissue-specific distribution. We also noticed that except IPA, *A. muciniphila* is able to consume oxindole and produce ILA, and indole-3-glycol aldehyde. Our previous studies also found that ILA effectively suppressed DOX-induced ferroptosis by activating AhR/Nrf2 signaling pathway to alleviate DIC[47]. These data indicated that tryptophan metabolites possess potent antioxidant activity and hold great potential in the treatment of cardiovascular diseases.

As IPA is an endogenous ligand for the AhR[48], we then hypothesize that its cardioprotective effects may be mediated through AhR binding. AhR is a cytoplasmic receptor and a highly conserved transcription factor. It is activated by various small-molecule ligands (such as natural products and host/gut microbiota), influencing a broad range of functions related to tissue homeostasis[49]. A substantial body of evidence indicates that AhR plays a crucial role in the development of cardiac fibrosis[50]. Tryptophan metabolism by the gut microbiota can mitigate cardiac fibrosis through the activation of the AhR signaling pathway[51]. Mitochondrial respiratory complexes, particularly Complex I and IV, have emerged as key regulators of cardiac function[52]. This study found that *A. muciniphila* colonization or IPA administration reversed the reduced expression of Ndufb8 and Atp5a protein caused by DOX, highlighting a promising therapeutic approach to DIC by regulating mitochondrial dynamics and energetic metabolism[53]. On the contrary, in mice with chronic kidney disease, AhR activation was inversely correlated with mitochondrial respiration[54] and knockout of AhR attenuates renal senescence and fibrosis, as well as the suppression of PGC1α-mediated mitochondrial biogenesis in ischemia reperfusion-induced kidneys[55]. These indicated that AhR activation showed differential cell-type-specific function. Moreover, Wang et al. found IPA binds AhR to promote the expression of SIRT3 and restore nicotinamide (NAM) and NAD+/NADH levels, attenuating oxidative stress and inflammation in the heart[22]. To the best of our knowledge, our study is the first to identify AhR as a regulator of mitochondrial OXPHOS, bioenergetics, and morphology, by regulating PPARα/PGC1α signaling pathway in the face of DIC. Taken together, the above studies indicated complex molecular mechanisms underlying the cardio-protective role of IPA (especially on mitochondria-mediated oxidative stress), and further studies are needed to dissect the signaling pathway underpinning IPA effects on cardio-protection.

Nevertheless, there are still limitations in this study. First, the mechanism by which AhR regulates PPARα in cardiomyocytes remains unclear, and further experiments (e.g., AhR knockout mice, transcription factor analysis, Co-IP) are required to elucidate the specific interactions between AhR and PPARα. Secondly, we acknowledge that antibiotic

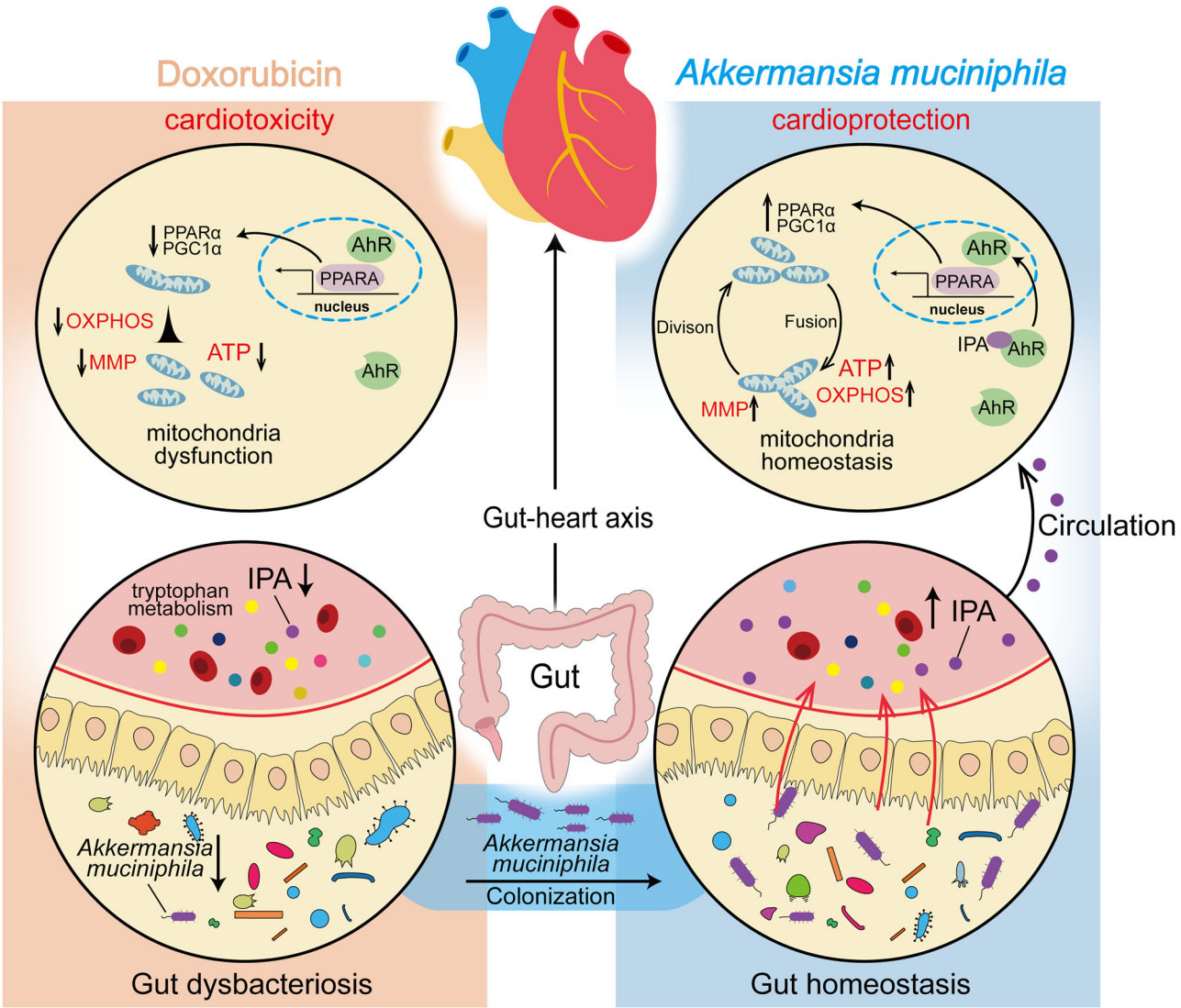

Fig. 9 | The schematic diagram of *Akkermansia muciniphila* (AKK) ameliorating doxorubicin (DOX)-induced cardiotoxicity. AKK colonization increased serum tryptophan metabolite indole-3-propionic acid (IPA), which improved DOX-induced mitochondrial dysfunction by activating cardiac aryl hydrocarbon receptor (AhR)-dependent PPARα/PGC1α signaling pathway, which could attenuate DOX-induced cardiotoxicity.

pretreatment does not fully eliminate microbial cross-talk. Future studies using germ-free models will be essential to definitively isolate *A. muciniphila*'s autonomous effects. Further studies are required to use FMT from DOX-treated patients to intervene in Abx mice or germ-free mice, thereby elucidating the critical role of *A. muciniphila* or gut microbiota in DIC. Ultimately, we observed that following *A. muciniphila* colonization, the abundance of Lactobacillus significantly decreased, and the IPA content in *A. muciniphila* supernatant was not the highest. Moreover, other types of gut microbiota species, including *Peptostreptococcus*[56] and *Clostridium sporogenes*[57], are also reported as producers of IPA. Consequently, it remains unclear how *A. muciniphila* influences other bacteria or regulates other metabolites to exert its cardioprotective effects. We will further investigate this question in our future research.

Overall, this study identified dysregulation in gut microbiota and tryptophan metabolism as a contributing factor to the progression of DIC. In our experiments, we treated DIC mice with *A. muciniphila* and found that *A. muciniphila* colonization effectively restored the balance of gut microbiota and tryptophan metabolism, thereby mitigating DOX-induced mitochondrial dysfunction. Mechanistically, *A. muciniphila* produces IPA, which binds to cardiac AhR and activates the PPARα/PGC1α signaling pathway, promoting mitochondrial bioenergetic metabolism (Fig. 9). This study demonstrates that *A. muciniphila* is an effective and safe probiotic therapy for protecting against DIC.

Methods

Study populations

Upon approval by the review of the Ethics Committee of the Shaoxing People's Hospital, we recruited 30 patients with breast cancer according to the following criteria: (1) diagnosed with breast cancer according to established diagnostic criteria; (2) age between 18 and 80 years; (3) demonstrates good treatment adherence and can follow medical advice. The exclusion criteria were: (1) patients diagnosed with tumors of other origins; (2) who suffer from severe primary diseases, including cardiovascular or cerebrovascular diseases, liver or kidney dysfunction, or hematopoietic system disorders; and (3) demonstrate poor treatment adherence, refuses treatment, or withdraws from the study. All enrolled patients underwent routine examinations before enrollment, and their daily diets were kept consistent. Serum and fecal samples were collected after the completion of chemotherapy. Patients were divided into nAC and AC groups based on the use of anthracycline drugs in the chemotherapy regimen. General clinical data

for all patients were collected, including tumor stage, chemotherapy regimen, cardiac function, and myocardial enzyme profiles. The clinical characteristics of patients are shown in Supplementary Table 1.

Animal studies

C57BL/6 mice (8 weeks old, weight from 18 to 25 g) were obtained from Genuine Biology Technology Co., Ltd. (Hangzhou, China) and were housed in the Animal Centre of Shaoxing People's Hospital and maintained under a 14-h light/8-h dark cycle at 24 °C with free access to chow and water.

Bacterial culture and treatment

A. muciniphila (Cat.B336076) was purchased from Mingzhoubio (Ningbo, China) and cultured anaerobically at 37 °C in Brain Heart Infusion media (MZM0089, Mingzhoubio). The samples were then resuspended to a concentration of 1×10^{10} colony-forming units (CFU)/mL PBS. Meanwhile, an equivalent amount of *A. muciniphila* was inactivated by pasteurization at 70 °C for 0.5 h. Antibiotic-pretreated (Abx-pretreated) mice were administered a 100-μL bacterial suspension (pasteurized *A. muciniphila* as a vehicle control) or 50 mg/kg benfluorex (Ben, an *A. muciniphila* inhibitor[14]) by gavage twice a week for 4 consecutive weeks.

Experimental groups

The flow chart for the experimental designs is demonstrated in the corresponding figures or Supplementary Materials. Six mice were randomly assigned to the following groups. Mice in the DIC group were established by receiving intraperitoneal injections of DOX at 5 mg/kg once a week for 4 weeks, reaching a cumulative dose of 20 mg/kg. Mice in the Abx group received a cocktail of Abx composed of ampicillin (400 mg/kg), neomycin (400 mg/kg), metronidazole (400 mg/kg), and vancomycin (200 mg/kg) daily for a continuous 5 days via gavage. Mice in the *A. muciniphila* group were administered (10^{10}) CFU of *A. muciniphila* in 100 μL PBS via gavage after 5 days of antibiotic treatment. Mice in the IPA groups received different concentrations of IPA via gavage. The stock solution of IPA (20 and 40 mg/kg, MedChemExpress) was made up in coin oil by the addition of 10% DMSO to fully resolve it. The dose of IPA was chosen based on previous studies[58–60] and our in vitro cell experiments. NXT629 (30 mg/kg)[18] and Ben (50 mg/kg)[14] were completely dissolved in sterile PBS and administered via oral gavage twice a week. To knockdown AhR, AAV9 carrying a cTNT promoter (pcAAV-cTNTo-EGFP-miR30 shRNA (AhR)-WPRE) or viral vector (pcAAV-cTNTo-EGFP-miR30 shRNA (NC)-WPRE) was purchased from Shanghai Obio Technology Co., Ltd. For cardiac delivery, 1×10^{11} particles of 100 μl (diluted in sterile PBS) were injected intravenously into mice.

Sample collection

Each mouse was individually placed on sterile gauze, and after being handled, the feces were promptly collected into sterile tubes using sterile forceps and immediately flash-frozen in liquid nitrogen for storage. Peripheral blood (1 mL) was collected from each mouse using the orbital blood collection method. The mice were then rapidly euthanized by cervical dislocation, immersed in 75% ethanol, the sternum was carefully dissected, and mouse hearts were rapidly harvested, rinsed in ice-cold PBS, and flash-frozen in liquid nitrogen. All samples were stored at −80 °C until testing.

Echocardiography

Mice were weighed before imaging and then anesthetized using a low-flow vaporizer (R500, RWD Life Science Co. Ltd., Sugar Land, USA) with ~2.5% isoflurane at 250 mL/min. Mice were then secured to a heated stage with gold-plated electrodes and had their ventral thorax hair removed using depilatory cream. Cardiac echocardiography was performed using the Vevo2100 system (Fujifilm visualsonics, Inc., Toronto, Canada) equipped with a 50-MHz center frequency transducer to measure parameters, including left ventricular (LV) ejection fraction (LVEF), LV fractional shortening (LVFS), LV internal dimension-systole (LVIDs), and LV internal dimension-diastole (LVIDd).

Histological assessment of myocardial injury and collagen content

H&E staining was used to evaluate the general morphology of the myocardium. The sections were imaged using the Leica DM3000 biological microscope (Leica, Wetzlar, Germany) at 200× magnification. Wheat germ agglutinin (WGA) staining was used to measure the DOX-induced myocardial atrophy. Sections were incubated with 5 μg/ml WGA (L4895; Sigma) solubilized in PBS for 20 min, at room temperature in the dark. After being washed three times with PBS, the sections were stained with DAPI (P36941; Invitrogen) and the images were acquired with a confocal microscope. The cardiac myocyte size was determined by the measurement of total area divided by the number of cardiac myocytes. For collagen analysis, the heart sections underwent Masson's trichrome staining. Collagen deposition was quantified using Image-ProPlus6 (Media Cybernetics, Rockville, USA).

Assessment of serum cardiac injury markers

Blood sample was centrifuged at 3000 rpm for 20 min to collect the plasma. The levels of CK-MB and LDH in plasma were measured by using commercialized kits (CK-MB (H197-1), LDH (A020-2), Nanjing Jiancheng Bioengineering Institute, China) using an auto-analyzer apparatus (Molecular Devices, CA), based on the manufacturer's protocols.

Transmission electron microscopy

The heart tissues were rapidly fixed in a solution containing 1.25% paraformaldehyde, 2.5% glutaraldehyde, and 0.03% picric acid. This was followed by osmication and uranyl acetate staining, dehydration in alcohols, and embedding in Araldite. The slides were then stained with toluidine blue. Ultrathin sections were cut from this block and observed under a Cs-corrected TEM with a Monochromator (Titan G2 60-300, FEI, Hillsboro).

Immunofluorescence staining

For immunofluorescence assays, sections were dewaxed, hydrated, and 0.01 mol/L hot citrate was used to repair the antigens of kidney tissue. The sections were subsequently stained sequentially with primary and secondary antibodies. After washed thrice after both primary and secondary antibody staining, the sections were counterstained with DAPI and images were captured using the confocal microscope.

Fecal microbiota composition

Total microbial genomic DNA was extracted using the Mag Bind DNA Kit (M9636-02, Omega Bio Tek). Following identification and purification, the V3-V4 variable regions were PCR-amplified, and the products were recovered from 2% agarose gel. The recovered products were then purified, quantified, and a library was constructed using the NEXTFLEX Rapid DNA-Seq Kit. Quality control was conducted with Fastp, and sequences were assembled using FLASH. OTU clustering of the quality-controlled sequences was performed based on 97% similarity.

Metabolomic profiling

Serum samples and stool samples from each mouse in this study were sent for metabolomic profiling by LC-Bio Technology CO., Ltd. using LC-MS/MS. Raw data were processed using TMBQ software, with peak integration, calibration, and quantification performed for each metabolite. Statistical analyses, including PCA, univariate analysis, and pathway analysis, were conducted using the custom-developed iMAP platform.

Transcriptome analysis of cardiac tissues

Total RNA was extracted from heart tissue using Trizol reagent (Invitrogen, Carlsbad, CA, USA). The RNA's quantity, purity, and integrity were assessed to ensure quality. For transcriptome analysis, total RNA (all with RIN numbers >7.0) was sequenced using 2×150 bp paired-end sequencing on an Illumina NovaSeq X Plus (LC-Bio Technology CO., Ltd, China). The expression levels of each transcript were quantified as fragments per kilobase of exon per million mapped reads (FPKM) using StringTie and Ballgown. Genes with a log2FC ≥ 1 and −log10P value ≥ 1.5 were considered significant.

Cell culture and cell viability assay

Isolation of primary NMVMs was obtained from neonatal mice (3–5 days old). Briefly, fresh hearts were placed into cold D-Hanks for washing, and hearts were minced into 1–3 mm^3 pieces and incubated with 3 mg/mL collagenase II (Sigma) in a 37 °C incubator for 90 min. After that, DMEM (Gibco) supplemented with 4.5 g/L glucose and 10% FBS was used for preparing a single-cell suspension by pipetting up and down. After incubation for another 90 min, fibroblasts were cleared so that cardiomyocytes were collected and then plated in DMEM with bromodeoxyuridine (BrdU, 100 μM, MedChemExpress). After being cultured for 24 h, NMVMs were used for experiments.

H9C2 cells (ATCC) were plated at 5000 cells/well in 96-well plates. Cell viability was estimated by a CCK-8 assay (MedChemExpress). Then cells were treated with vehicle (DMSO), IPA (1–1000 μm), GNF351 (500 nM) in the presence or absence of 1 μg/mL of DOX for 24 h. At the end of the 24 h, the medium was removed, and the new medium with 10 μL CCK-8 agent was added to each well for another 2 h. The absorbance was measured at 450 nm in an enzyme labeling.

Probes for mitochondrial detection

The morphology of mitochondria was assessed using MitoTracker Red CMXRos staining (C1035, Beyotime) in H9C2 cells. Cells were observed using a confocal microscope (Leica, Germany) at a ×63 objective. To assess mitochondrial morphological changes, 4 independent experiments were conducted, with 20 cells randomly selected under the microscope for area measurement in each experiment.

Assessment of mitochondrial function

Mitochondria were isolated from heart tissue blocks following the protocol provided with the detection kits (C3606, Beyotime). The activities of mitochondrial complexes I, II, III, IV, and V were measured spectrophotometrically using specific detection kits: complex I (Cat. abs580238) at 340 nm, complex II (Cat. abs580239) at 605 nm, complex III (Cat. abs580240) and complex IV (Cat. abs580241) at 550 nm, and complex V at 340 nm (abs580242, Absin, Shanghai, China), all according to the manufacturer's instructions.

Oxygen consumption rate (OCR) was measured using a Seahorse XF96 analyzer (Agilent, Santa Clara, CA, USA) following the manufacturer's instructions. NMVMs were seeded into XFe96 plates at an appropriate density. OCR was measured using the Seahorse XF Cell Mitochondrial Stress Test (103015–100; Agilent). After baseline OCR recording, oligomycin, trifluoromethoxy carbonylcyanide phenylhydrazone (FCCP), and a combination of rotenone and antimycin A were sequentially added to assess ATP-coupled respiration, maximal respiration, and non-mitochondrial respiration. NMVMs or H9C2 cells were plated in 96 wells at 5000 cells/well and cultured overnight. The ATP determination was performed with an ATP determination kit (Invitrogen).

The mitochondrial membrane potential (MMP) was assessed through the JC-1 MMP detection kit (MedChemExpress, Shanghai, China) following the manufacturer's instructions. Briefly, treated H9C2 cells were incubated with JC-1 for 30 min at 37 °C in the dark, and the images were taken with a confocal microscope.

RNA extraction and quantitative PCR

Total RNA was extracted using Trizol (Invitrogen, Carlsbad, CA), and reverse transcription was performed with the PrimeScript RT reagent kit (Takara). mRNA expression levels were quantified by real-time PCR using the SYBR Premix Ex Taq kit on a Roche LightCycler 480 system (Roche Diagnostics, IN, USA). The primers used for mRNA detection were listed in Supplementary Table 2. The results were analyzed using the $2^{-\Delta\Delta Ct}$ method.

To determine the abundance of bacteria, genomic DNA was extracted from fecal samples using the Fecal Genome DNA Extraction Kit (TIANGEN; #DP328). The extracted DNA was then precipitated by centrifugation at 12,000 × *g* for 2 min in a microcentrifuge. Following precipitation, the DNA was washed with 70% ethanol and resuspended in nuclease-free water. The genomic DNA of *A. muciniphila* was used to establish a standard curve via RT-qPCR. The SYBR Green Realtime PCR Master Mix (QPK-201, TOYOBO) was employed for the qPCR reactions. The reaction conditions consisted of an initial denaturation at 95 °C for 30 s, followed by 40 cycles of amplification: 95 °C for 5 s, 60 °C for 10 s, and 72 °C for 15 s. Various concentrations of genomic DNA were used as templates to obtain corresponding Ct values.

Western blot analysis

Protein samples were extracted from mouse hearts, NMVMs, or H9C2 cells and separated using SDS-PAGE. The proteins were then transferred onto PVDF membranes (Sigma). The membranes were blocked for 5 min at room temperature using a protein-free rapid sealing solution (G2052, Servicebio, Wuhan, China), followed by overnight incubation at 4 °C with the specified primary antibodies. After washing, the membranes were incubated with secondary antibodies for 1 h at room temperature. Bands were visualized using an ECL kit (Beyotime, Jiangsu, China), and protein levels were quantified with ImageJ software. Relative protein expression, normalized to GAPDH, was displayed. The information on antibodies was listed in Supplementary Table 3.

Statistical analysis

Statistical analysis for the main and Supplementary Figures was conducted using GraphPad Prism versions 9 and 10. Significance was assessed with either an unpaired, two-tailed Student's *t* test or a one-way analysis of variance (ANOVA) followed by the SNK multiple comparisons test for post hoc analysis. Normality was checked using the Shapiro–Wilk test before applying parametric statistics. For groups with unequal variances, *t* tests or ANOVA with Welch's correction were used. For non-normal distributions, the Mann–Whitney or Kruskal–Wallis test was employed. *P* value <0.05 was considered statistically significant. Error bars indicate SD (standard deviation) unless stated otherwise.

Data availability

All data used in this study are present in the main text and Supplementary Materials. The 16S RNA data have been deposited in the NCBI Sequence Read Archive (SRA) database (accession numbers: PRJNA1151312 and PRJNA1152730). RNA-seq data of mouse hearts were deposited at NCBI (accession number: GSE276172). All original data in this study are deposited in Mendeley Data, V1, doi: 10.17632/dk8hw2m7gg.1.

Received: 9 October 2024; Accepted: 26 April 2025;
Published online: 23 May 2025

References

1. Magdy, T. et al. Identification of drug transporter genomic variants and inhibitors that protect against doxorubicin-induced cardiotoxicity. *Circulation* **145**, 279–294 (2022).
2. Qiao, X. et al. Diversifying the anthracycline class of anti-cancer drugs identifies aclarubicin for superior survival of acute myeloid leukemia patients. *Mol. Cancer* **23**, 120 (2024).
3. Vitale, R., Marzocco, S. & Popolo, A. Role of oxidative stress and inflammation in doxorubicin-induced cardiotoxicity: a brief account. *Int. J. Mol. Sci.* **25**, 7477 (2024).
4. Wu, L., Wang, L., Du, Y., Zhang, Y. & Ren, J. Mitochondrial quality control mechanisms as therapeutic targets in doxorubicin-induced cardiotoxicity. *Trends Pharm. Sci.* **44**, 34–49 (2023).
5. Antoniak, S. et al. Protease-activated receptor 1 activation enhances doxorubicin-induced cardiotoxicity. *J. Mol. Cell Cardiol.* **122**, 80–87 (2018).
6. Ghionzoli, N. et al. Current and emerging drug targets in heart failure treatment. *Heart Fail. Rev.* **27**, 1119–1136 (2022).
7. Di Modica, M. et al. Gut microbiota condition the therapeutic efficacy of trastuzumab in HER2-positive breast cancer. *Cancer Res.* **81**, 2195–2206 (2021).

8. Bawaneh, A. et al. Intestinal microbiota influence doxorubicin responsiveness in triple-negative breast cancer. *Cancers* https://doi.org/10.3390/cancers14194849 (2022).
9. An, L., Wuri, J., Zheng, Z., Li, W. & Yan, T. Microbiota modulate doxorubicin induced cardiotoxicity. *Eur. J. Pharm. Sci.* **166**, 105977 (2021).
10. Zhou, J. et al. Fecal microbiota transplantation in mice exerts a protective effect against doxorubicin-induced cardiac toxicity by regulating Nrf2-mediated cardiac mitochondrial fission and fusion. *Antioxid. Redox Signal.* **41**, 1–23 (2024).
11. Huang, J. et al. Involvement of abnormal gut microbiota composition and function in doxorubicin-induced cardiotoxicity. *Front. Cell Infect. Microbiol.* **12**, 808837 (2022).
12. Huang, C. et al. Role of gut microbiota in doxorubicin-induced cardiotoxicity: from pathogenesis to related interventions. *J. Transl. Med.* **22**, 433 (2024).
13. Lin, H. et al. Yellow wine polyphenolic compound protects against doxorubicin-induced cardiotoxicity by modulating the composition and metabolic function of the gut microbiota. *Circ. Heart Fail.* **14**, e008220 (2021).
14. Nie, Q. et al. Gut symbionts alleviate MASH through a secondary bile acid biosynthetic pathway. *Cell* **187**, 2717.e3–2734.e3 (2024).
15. Yu, S. et al. Time of exercise differentially impacts bone growth in mice. *Nat. Metab.* https://doi.org/10.1038/s42255-024-01057-0 (2024).
16. Lee, T.-W. et al. PPARs modulate cardiac metabolism and mitochondrial function in diabetes. *J. Biomed. Sci.* **24**, 5 (2017).
17. Wójtowicz, S., Strosznajder, A. K., Jeżyna, M. & Strosznajder, J. B. The novel role of PPAR alpha in the brain: promising target in therapy of Alzheimer's disease and other neurodegenerative disorders. *Neurochem. Res.* **45**, 972–988 (2020).
18. Stebbins, K. J. et al. In vitro and in vivo pharmacology of NXT629, a novel and selective PPARα antagonist. *Eur. J. Pharmacol.* **809**, 130–140 (2017).
19. Wang, G. et al. Microbiota-derived indoles alleviate intestinal inflammation and modulate microbiome by microbial cross-feeding. *Microbiome* **12**, 59 (2024).
20. Du, Y. et al. Live and pasteurized *Akkermansia muciniphila* ameliorates diabetic cognitive impairment by modulating gut microbiota and metabolites in db/db mice. *Exp. Neurol.* **378**, 114823 (2024).
21. Wang, Y. et al. Unraveling the differential perturbations of species-level functional profiling of gut microbiota among phases of methamphetamine-induced conditioned place preference. *Prog. Neuropsychopharmacol. Biol. Psychiatry* **127**, 110828 (2023).
22. Wang, Y. C. et al. Indole-3-propionic acid protects against heart failure with preserved ejection fraction. *Circ. Res.* **134**, 371–389 (2024).
23. Kretzschmar, T. et al. Metabolic profiling identifies 1-MetHis and 3-IPA as potential diagnostic biomarkers for patients with acute and chronic heart failure with reduced ejection fraction. *Circ. Heart Fail.* **17**, e010813 (2024).
24. Zhang, L. S. & Davies, S. S. Microbial metabolism of dietary components to bioactive metabolites: opportunities for new therapeutic interventions. *Genome Med.* **8**, 46 (2016).
25. Rothhammer, V. et al. Type I interferons and microbial metabolites of tryptophan modulate astrocyte activity and central nervous system inflammation via the aryl hydrocarbon receptor. *Nat. Med.* **22**, 586–597 (2016).
26. Bi, Y. et al. Aryl hydrocarbon receptor nuclear translocator limits the recruitment and function of regulatory neutrophils against colorectal cancer by regulating the gut microbiota. *J. Exp. Clin. Cancer Res.* **42**, 53 (2023).
27. Grander, C. et al. Recovery of ethanol-induced *Akkermansia muciniphila* depletion ameliorates alcoholic liver disease. *Gut* **67**, 891–901 (2018).
28. Mruk-Mazurkiewicz, H. et al. Insights into the mechanisms of action of *Akkermansia muciniphila* in the treatment of non-communicable diseases. *Nutrients* https://doi.org/10.3390/nu16111695 (2024).
29. Niu, H. et al. *Akkermansia muciniphila*: a potential candidate for ameliorating metabolic diseases. *Front. Immunol.* **15**, 1370658 (2024).
30. He, X., Bai, Y., Zhou, H. & Wu, K. *Akkermansia muciniphila* alters gut microbiota and immune system to improve cardiovascular diseases in murine model. *Front. Microbiol.* **13**, 906920 (2022).
31. Luo, Y. et al. *Akkermansia muciniphila* prevents cold-related atrial fibrillation in rats by modulation of TMAO induced cardiac pyroptosis. *EBioMedicine* **82**, 104087 (2022).
32. Li, J., Lin, S., Vanhoutte, P. M., Woo, C. W. & Xu, A. *Akkermansia Muciniphila* protects against atherosclerosis by preventing metabolic endotoxemia-induced inflammation in Apoe-/- mice. *Circulation* **133**, 2434–2446 (2016).
33. Wang, J. et al. *Akkermansia muciniphila* participates in the host protection against helminth-induced cardiac fibrosis via TLR2. *PLoS Pathog.* **19**, e1011683 (2023).
34. Zhu, S. G. et al. Dietary nitrate supplementation protects against doxorubicin-induced cardiomyopathy by improving mitochondrial function. *J. Am. Coll. Cardiol.* **57**, 2181–2189 (2011).
35. Montaigne, D., Butruille, L. & Staels, B. PPAR control of metabolism and cardiovascular functions. *Nat. Rev. Cardiol.* **18**, 809–823 (2021).
36. Roy, A. et al. Regulation of cyclic AMP response element binding and hippocampal plasticity-related genes by peroxisome proliferator-activated receptor α. *Cell Rep.* **4**, 724–737 (2013).
37. Francque, S. et al. PPARα gene expression correlates with severity and histological treatment response in patients with non-alcoholic steatohepatitis. *J. Hepatol.* **63**, 164–173 (2015).
38. Xu, H. et al. Aged microbiota exacerbates cardiac failure by PPARα/PGC1α pathway. *Biochim. Biophys. Acta Mol. Basis Dis.* **1870**, 167271 (2024).
39. Du, L. et al. Therapeutic potential of ginsenoside Rb1-PLGA nanoparticles for heart failure treatment via the ROS/PPARα/PGC1α pathway. *Molecules* https://doi.org/10.3390/molecules28248118 (2023).
40. Mujagic, Z. et al. Integrated fecal microbiome-metabolome signatures reflect stress and serotonin metabolism in irritable bowel syndrome. *Gut Microbes* **14**, 2063016 (2022).
41. Zhao, J. et al. Heart-gut microbiota communication determines the severity of cardiac injury after myocardial ischaemia/reperfusion. *Cardiovasc. Res.* **119**, 1390–1402 (2023).
42. Jiang, Z. M. et al. *Hypericum perforatum* L. attenuates depression by regulating *Akkermansia muciniphila*, tryptophan metabolism and NFκB-NLRP2-Caspase1-IL1β pathway. *Phytomedicine* **132**, 155847 (2024).
43. Pan, M. et al. Gut-derived lactic acid enhances tryptophan to 5-hydroxytryptamine in regulation of anxiety via *Akkermansia muciniphila*. *Gut Microbes* **17**, 2447834 (2025).
44. Alvarado, D. M. et al. Epithelial indoleamine 2,3-dioxygenase 1 modulates aryl hydrocarbon receptor and Notch signaling to increase differentiation of secretory cells and alter mucus-associated microbiota. *Gastroenterology* **157**, 1093.e1–1108.e1 (2019).
45. Agus, A., Planchais, J. & Sokol, H. Gut microbiota regulation of tryptophan metabolism in health and disease. *Cell Host Microbe* **23**, 716–724 (2018).
46. Barroso, A., Mahler, J. V., Fonseca-Castro, P. H. & Quintana, F. J. The aryl hydrocarbon receptor and the gut-brain axis. *Cell. Mol. Immunol.* **18**, 259–268 (2021).
47. Lian, J. et al. Indole-3-lactic acid inhibits doxorubicin-induced ferroptosis through activating aryl hydrocarbon receptor/Nrf2 signalling pathway. *J. Cell Mol. Med.* **29**, e70358 (2025).
48. Chen, C. et al. Microbial tryptophan metabolites ameliorate ovariectomy-induced bone loss by repairing intestinal AhR-mediated gut-bone signaling pathway. *Adv. Sci.***11**, e2404545 (2024).

49. Yang, C. E. et al. Aryl hydrocarbon receptor: from pathogenesis to therapeutic targets in aging-related tissue fibrosis. *Ageing Res. Rev.* **79**, 101662 (2022).
50. Melhem, N. J. et al. Endothelial cell indoleamine 2, 3-dioxygenase 1 alters cardiac function after myocardial infarction through kynurenine. *Circulation* **143**, 566–580 (2021).
51. Carrillo-Salinas, F. J. et al. Gut dysbiosis induced by cardiac pressure overload enhances adverse cardiac remodeling in a T cell-dependent manner. *Gut Microbes* **12**, 1–20 (2020).
52. Hinton, A. Jr. et al. Mitochondrial structure and function in human heart failure. *Circ. Res.* **135**, 372–396 (2024).
53. Yang, M. et al. PHB2 ameliorates doxorubicin-induced cardiomyopathy through interaction with NDUFV2 and restoration of mitochondrial complex I function. *Redox Biol.* **65**, 102812 (2023).
54. Thome, T. et al. A tryptophan-derived uremic metabolite/Ahr/Pdk4 axis governs skeletal muscle mitochondrial energetics in chronic kidney disease. *JCI Insight* https://doi.org/10.1172/jci.insight.178372 (2024).
55. Xie, H. et al. Uremic toxin receptor AhR facilitates renal senescence and fibrosis via suppressing mitochondrial biogenesis. *Adv. Sci.* **11**, e2402066 (2024).
56. Roager, H. M. & Licht, T. R. Microbial tryptophan catabolites in health and disease. *Nat. Commun.* **9**, 3294 (2018).
57. Krause, F. F. et al. Clostridium sporogenes-derived metabolites protect mice against colonic inflammation. *Gut Microbes* **16**, 2412669 (2024).
58. Heumel, S. et al. Shotgun metagenomics and systemic targeted metabolomics highlight indole-3-propionic acid as a protective gut microbial metabolite against influenza infection. *Gut Microbes* **16**, 2325067 (2024).
59. Zeng, Y. et al. Gut microbiota-derived indole-3-propionic acid alleviates diabetic kidney disease through its mitochondrial protective effect via reducing ubiquitination mediated-degradation of SIRT1. *J. Adv. Res.* https://doi.org/10.1016/j.jare.2024.08.018 (2024).
60. Wang, Z. et al. The gut microbiota-derived metabolite indole-3-propionic acid enhances leptin sensitivity by targeting STAT3 against diet-induced obesity. *Clin. Transl. Med.* **14**, e70053 (2024).

Acknowledgements

This work was supported by grants from the National Natural Science Foundation of China (Grant Nos. 82200390, 82000252, 82300347 and 81870255), Zhejiang Provincial Natural Science Foundation of China (Grant Nos. ZCLTGD24H0201 and LHDMZ24H020001), Medical Health Science and Technology Project of Zhejiang Provincial (2022RC079, 2022KY1303, and 2024KY528), Ningbo Key Laboratory of Molecular Target Screening and Application (grant No. 2023-BZDS), Ningbo Key Research and Development Program (grant No. 2024Z210), Key Specialized Construction Project in Cardiology Department of Zhejiang Province (2023-SZZ), and the Science and Technology Projects of Shaoxing city (Grant Nos. 2022A14009 and 2023A14011).

Author contributions

H.L., J.L., J.C., and L.M. conceived and designed the study. H.L., H.G., X.Y., Z.Z., D.L., F.C., Y.S., and X.S. performed the experiments. X.Y., F.C., Y.S., P.W., X.S., S.G., and L.M. performed the data analysis and bioinformatics analysis. J.L., J.C., X.S., and L.M. supervised and funded the project. H.L., H.G., X.Y., Z.Z., Y.S., and L.M. wrote the draft manuscript. H.L., X.Y., H.L., Z.Z., X.S., and L.M. revised the manuscript. All authors contributed to the article and approved the submitted version.

Competing interests

The authors declare no competing interests.

Ethics approval and consent to participate

All the participants provided written informed consent. All human experiments followed a protocol (2024084-01) approved by the Medical Ethics Committee of Shaoxing People's Hospital. The experimental procedures were approved by the Institutional Animal Care and Use Committee of Shaoxing People's Hospital (NO.2022002).

Additional information

Supplementary information The online version contains supplementary material available at https://doi.org/10.1038/s41522-025-00712-y.

Correspondence and requests for materials should be addressed to Liping Meng, Jufang Chi or Jiangfang Lian.